Free vibration analysis of functionally graded carbon nanotubes reinforced double plates

Free vibration analysis of functionally graded carbon nanotubes reinforced double plates

Oscar Zi Shao Ong[a,*], Mergen H. Ghayesh[a], Nicholas Fantuzzi[b], Krzysztof Kamil Żur[c]

[a]*School of Electrical and Mechanical Engineering, University of Adelaide, Adelaide, South Australia, Australia*

[b]*DICAM – Department, School of Engineering and Architecture, University of Bologna, Italy*

[c]*Faculty of Mechanical Engineering, Bialystok University of Technology, 15-351 Bialystok, Poland*

[*]*corresponding author: oscarzishao.ong@adelaide.edu.au*

Abstract

The specific objective of this study is to analyse the dynamics of functionally graded carbon nanotubes reinforced double plates. Connected via an elastic layer, the plates have simply supported boundary conditions. Three carbon nanotubes functionally graded patterns, varying in the thickness direction are considered in the current study, including uniformly distributed, functionally graded O pattern, and functionally graded X pattern. Following the development of the coupled equations of motion using the Hamilton principle while considering the influences of the elastic layer, the equations are subsequently solved utilising a two-spatial-variable modal decomposition method. For verification purposes, the equations developed are compared to simplified configurations provided in existing studies. The solution methodology is verified through comparing against numerical results of simplified configurations of plates obtained from the development of the finite element method (FEM) and existing studies. Both verifications have shown very good agreement. Influences of plates' dimensions, carbon nanotubes reinforcement and the stiffness of elastic layer are analysed and provided in this study. The transverse-motion natural frequencies of the double plates are also identified, and they follow a decreasing trend as the aspect ratio increases for all the cases. The fundamental lateral-motion and axial-motion natural frequency also follow a similar trend as the aspect ratio increases. The reinforcement effect of carbon nanotubes on the transverse-motion natural frequencies is less obvious for thinner plates. An increase in the elastic layer stiffness increases the second series transverse-motion natural frequencies of the double-plate system. Among the considered functionally graded patterns, the FG-X reinforcement provides the largest increase in the transverse-motion natural frequencies.

keywords: *double plates; elastic layer; Kirchhoff's plate theory; carbon nanotubes reinforced; FGCNT.*

1. Introduction

Simple or intricate two-dimensional continuous systems like shells and plates are commonly employed to model the majority of mechanical structures utilised in different engineering fields [1]. Plates especially are popular across various engineering domains such as civil, mechanical and automotive engineering disciplines [2].

Over the past few decades, numerous research has been carried out to address the challenges posed by the dynamical issues of *single isotropic* plates [3-5]. One of the recent examples is Karimi, Alahdadi and Ghayour [6]'s work, where they focused on the dynamics of a thin plate with a moving mass. It was concluded that plate's deflection has a considerable effect on the mass motion. Furthermore, Zhang et al. [7] investigated the vibrations of a skewed rotating plate. Their modelling results suggest the non-uniform centrifugal force could cause the skewed plate to buckle. Exciting a plate using a travelling oscillator, Foyouzat [8] examined the dynamics of the system. The results suggest the response of the plate is mostly less sensitive to the assumed restitution coefficient. Moreover, Kubiak, Borkowski and Perlikowski [9] investigated the dynamics of a plate when either a pulsating or harmonic load is acting on it.

Complex structures can be fabricated by combining at least two materials with distinct properties, giving rise to a new form of materials, namely composite [10-20]. A subclass of composite is functionally graded materials [21-25], made possible by additive manufacturing [26], where the material properties vary in a continuous manner as the material changes [27]. This makes functionally graded material superior because it solves the problem of stress concentrations which led to wide application in biomedical field and sports [28]. There has also been a large number of studies carried out in the area of dynamics of functionally graded plates [29-36]. For example, Hoang and Thanh [37] studied the influences of the Kerr foundation and thermal environment on the dynamics of a functionally graded plate. Their study indicates that the increase in temperature causes a decrease in the natural frequency of the plate. Rajasekaran, Khaniki and Ghayesh [38] investigated the dynamics of a functionally graded plate that is multi-layer multi-directional in a thermal environment. The results show that the natural frequency decreases as the power law term increases.

Discovered by Iijima [39] and made by rolling a graphite sheet into a tube, carbon nanotubes are a promising new material to act as a reinforcement [40-42]. Carbon nanotubes are extremely strong and lightweight, and they have excellent electrical and thermal conductivity [43]. These properties make them well-suited for use in reinforcing plates that are subjected to high loads

or that need to conduct heat away from a source. There is also a plethora of research into carbon nanotubes reinforced plates [44-50]. Kumar and Jana [51], for instance, focused on the dynamics of a carbon nanotubes reinforced laminated plate in their studies. They found that when the carbon nanotubes are distributed around the edges of the plate, the natural frequency of the system is higher than the plate with carbon nanotubes in the middle. Dat et al. [52] studied the vibrations of a functionally graded carbon nanotubes reinforced multilayered plate with a porous core. The research found that the carbon nanotubes volume fraction reduces the vibrations of the system. Interested readers to the topic of carbon nanotubes reinforced structures may see a recent review paper by Khaniki and Ghayesh [53].

Consisting of two plates, a *double plated* structure has gained extensive utilisation in various engineering fields, including construction due to their notable effectiveness in noise reduction and vibration isolation. Examples of applications include the utilisation in the creation of the bulkhead within the hull structure, and the integration into double-layer sound insulation panels [54]. In practical engineering, elastic connections are frequently employed to connect the double plates in order to enhance their mechanical properties. The presence of elastic structures alters the vibrational behaviour of the original *isotropic non*-reinforced double plated structure, garnering significant interest from researchers. Oniszczuk [55] first investigated the free vibrations of double plates connected via an elastic layer using the Kirchhoff-Love plate theory and the classical Navier method. The data suggest that the free vibrations of the system is similar to a double membrane system in some aspects. Oniszczuk [56] then expanded the study to investigate the forced vibrations of a double plates system. Wen et al. [57] modelled the vibrational behaviour of double plates which consist of inner fluids and elastic layer. They concluded that the inner air reduces the transmission of vibrations between the plates. Cao et al. [58] investigated the dynamics of viscoelastically connected double plates with moving loads. While not considering damping, they found that double plates' deformations are symmetric and the displacements increase as the moving load velocity increases. Increasing the numbers of plates beyond two, Heidari and Ariaei [59] proposed a new approach for the free vibrations of the multiple elastically connected plates. They found the prominence of the elastic layer effects becomes smaller as the order of modes increases.

It is now well established that the dynamics of a carbon nanotubes reinforced and non-reinforced *single* plate, and the dynamics of *non*-reinforced *double* plates using the Kirchhoff plate theory are well investigated. However, the influence of *carbon nanotubes* on the dynamics of *double plates* has remained unclear. Expanding on the prior investigations, this

study represents the first free vibration analysis of functionally graded carbon nanotubes reinforced rectangular double plates, connected via an elastic layer, with simply supported boundary conditions. The carbon nanotubes are arranged in the thickness direction. Three different functionally graded patterns are considered, namely uniformly distributed, FG-O and FG-X. To formulate the equations of motion, the kinetic and potential energies are first formulated after considering the Kirchhoff plate theory. The final equations are then obtained by applying the Hamilton principle and solved using the two-spatial variable modal decomposition method (MDM). The equations are verified with simplified versions of the system under investigation that have been previously studied. Similarly, the numerical results are verified using the simplified models from existing literature. A simplified version of the proposed system is also simulated using the finite element method (FEM), and the numerical results obtained using both the methods are compared to verify the accuracy of the proposed methodology. This study investigates in details the effects of plates' aspect ratios, plates' thicknesses, the carbon nanotubes functionally graded patterns and the elastic layer stiffness.

2. Model development and solution methodology

This section models the dynamics of simply supported functionally graded carbon nanotubes reinforced rectangular double plates. The plates are connected through an elastic layer with a stiffness coefficient of k, per unit area. Plates 1 (top) and 2 (bottom) with a thickness of h_1 and h_2, in-plane dimensions of a_1, a_2, b_1, and b_2 in the x (axial) and y (lateral) directions, are shown in Fig. 1(a).

2.1. Carbon nanotubes reinforced plates

The carbon nanotubes are distributed along the z-axis (out-of-plane coordinate), which is in the thickness (i.e. transverse) direction of both the plates. Their volume fraction, V_{CNT}, is dependent on V_{CNT}^{*}. As shown in Fig. 1(b), the three carbon nanotubes reinforcement patterns employed for the double plates are

(1) Uniformly distributed (UD)

The surfaces of the carbon nanotubes reinforced plates maintain an equal volume fraction of carbon nanotubes throughout its thickness. The volume fraction is formulated as [60]

$$V_{CNT}\left(z\right)=V_{CNT}^{*};\tag{1a}$$

(2) Functionally graded O-pattern (FG-O)

With an O-pattern, the top and bottom plates surfaces do not contain carbon nanotubes, while the mid-surface of the panel has an increased concentration of carbon nanotubes. The formulation for the volume fraction is expressed as [61]

$$V_{CNT}\left(z\right)=\left(\frac{2h-4\left|z\right|}{h}\right)V_{CNT}^{*};\tag{1b}$$

(3) Functionally graded X-pattern (FG-X)

The distribution of carbon nanotubes is concentrated near the top and bottom surfaces, while the mid-plane has no carbon nanotubes, resulting in an X-shape. The volume fraction is defined by the following formulation [62]

$$V_{CNT}\left(z\right)=\frac{4}{h}\left|z\right|V_{CNT}^{*}.\tag{1c}$$

The volume fractions of the carbon nanotubes are also related to the volume fraction of the matrix, V_m, through

$$\begin{aligned}&V_{1CNT}\left(z_1\right)=1-V_{1m}\left(z_1\right),\\&V_{2CNT}\left(z_2\right)=1-V_{2m}\left(z_2\right).\end{aligned}\tag{2}$$

The final material properties (Young's modulus, shear modulus, Poisson's ratio and density) of plates 1 and 2 are dependent on the carbon nanotubes reinforcement efficiency, η. The volume fraction employed in the current study with their corresponding carbon nanotubes reinforcement efficiency are [63, 64]

$$\begin{aligned}&\text{when } V_{CNT}^{*}=0.11,\\&\eta_1=0.149,\ \eta_2=0.934;\\&\text{when } V_{CNT}^{*}=0.14,\\&\eta_1=0.150,\ \eta_2=0.941;\\&\text{when } V_{CNT}^{*}=0.17,\\&\eta_1=0.149,\ \eta_2=1.381;\\&\text{for all } V_{CNT}^{*},\ \eta_2=\eta_3.\end{aligned}\tag{3}$$

Based on the rule of mixture, the material properties are [60]

$$
\begin{aligned}
&E_{111}(z_1)=\eta_{11}E_{111CNT}V_{1CNT}(z_1)+E_{1m}V_{1m}(z_1),\\
&E_{211}(z_2)=\eta_{21}E_{211CNT}V_{2CNT}(z_2)+E_{2m}V_{2m}(z_2),\\
&\frac{\eta_{12}}{E_{122}(z_1)}=\frac{V_{1CNT}(z_1)}{E_{122CNT}}+\frac{V_{1m}(z_1)}{E_{1m}},\ \frac{\eta_{22}}{E_{222}(z_2)}=\frac{V_{2CNT}(z_2)}{E_{222CNT}}+\frac{V_{2m}(z_2)}{E_{2m}},\\
&\frac{\eta_{13}}{G_{112}(z_1)}=\frac{V_{1CNT}(z_1)}{G_{112CNT}}+\frac{V_{1m}(z_1)}{G_{1m}},\ \frac{\eta_{23}}{G_{212}(z_2)}=\frac{V_{2CNT}(z_2)}{G_{212CNT}}+\frac{V_{2m}(z_2)}{G_{2m}},\\
&\nu_{112}(z_1)=(\nu_{112CNT}-\nu_{1m})V_{1CNT}(z_1)+\nu_{1m},\ \nu_{212}(z_2)=(\nu_{212CNT}-\nu_{2m})V_{2CNT}(z_2)+\nu_{2m},\\
&\nu_{121}(z_1)=\frac{\nu_{112}(z_1)}{E_{111}(z_1)}E_{122}(z_1),\ \nu_{221}(z_2)=\frac{\nu_{212}(z_2)}{E_{211}(z_2)}E_{222}(z_2),\\
&\rho_1(z_1)=\rho_{1CNT}V_{1CNT}(z_1)+\rho_{1m}V_{1m}(z_1),\\
&\rho_2(z_2)=\rho_{2CNT}V_{2CNT}(z_2)+\rho_{2m}V_{2m}(z_2).
\end{aligned}
\tag{4}
$$

2.2. Equations of motion

Based on the Kirchhoff plate theory, the strains of the carbon nanotubes reinforced double plates with elastic layer can be formulated as follows [65]

$$
\begin{aligned}
&\varepsilon_{1xx}=\frac{\partial u_1}{\partial x_1}-z_1\frac{\partial^2 w_1}{\partial x_1^2},\\
&\varepsilon_{1yy}=\frac{\partial v_1}{\partial y_1}-z_1\frac{\partial^2 w_1}{\partial y_1^2},\\
&\varepsilon_{1xy}=\frac{1}{2}\left(\frac{\partial u_1}{\partial y_1}-2z_1\frac{\partial^2 w_1}{\partial x_1\partial y_1}+\frac{\partial v_1}{\partial x_1}\right),\\
&\varepsilon_{2xx}=\frac{\partial u_2}{\partial x_2}-z_2\frac{\partial^2 w_2}{\partial x_2^2},\\
&\varepsilon_{2yy}=\frac{\partial v_2}{\partial y_2}-z_2\frac{\partial^2 w_2}{\partial y_2^2},\\
&\varepsilon_{2xy}=\frac{1}{2}\left(\frac{\partial u_2}{\partial y_2}-2z_2\frac{\partial^2 w_2}{\partial x_2\partial y_2}+\frac{\partial v_2}{\partial x_2}\right).
\end{aligned}
\tag{5}
$$

Double plates' displacements field are specified within a Cartesian coordinate system and the mid-plane coordinates are established using the *x* and *y* axes. The displacements of individual points on the mid-plane of the plates in the *x*, *y*, and *z* directions from the static equilibrium ($u = v = w = 0$) are represented by $u = u(x, y, t)$, $v = v(x, y, t)$, and $w = w(x, y, t)$, respectively. The variable *t* denotes time.

The stresses can then be written as [65]

$$
\begin{aligned}
\sigma_{1xx} &= Q_{111}\left(\frac{\partial u_1}{\partial x_1} - z_1\frac{\partial^2 w_1}{\partial x_1^2}\right) + Q_{112}\left(\frac{\partial v_1}{\partial y_1} - z_1\frac{\partial^2 w_1}{\partial y_1^2}\right),\\
\sigma_{1yy} &= Q_{122}\left(\frac{\partial v_1}{\partial y_1} - z_1\frac{\partial^2 w_1}{\partial y_1^2}\right) + Q_{112}\left(\frac{\partial u_1}{\partial x_1} - z_1\frac{\partial^2 w_1}{\partial x_1^2}\right),\\
\sigma_{1xy} &= G_{112}\left(\frac{\partial u_1}{\partial y_1} - 2z_1\frac{\partial^2 w_1}{\partial x_1\partial y_1} + \frac{\partial v_1}{\partial x_1}\right),\\
\sigma_{2xx} &= Q_{211}\left(\frac{\partial u_2}{\partial x_2} - z_2\frac{\partial^2 w_2}{\partial x_2^2}\right) + Q_{212}\left(\frac{\partial v_2}{\partial y_2} - z_2\frac{\partial^2 w_2}{\partial y_2^2}\right),\\
\sigma_{2yy} &= Q_{222}\left(\frac{\partial v_2}{\partial y_2} - z_2\frac{\partial^2 w_2}{\partial y_2^2}\right) + Q_{212}\left(\frac{\partial u_2}{\partial x_2} - z_2\frac{\partial^2 w_2}{\partial x_2^2}\right),\\
\sigma_{2xy} &= G_{212}\left(\frac{\partial u_2}{\partial y_2} - 2z_2\frac{\partial^2 w_2}{\partial x_2\partial y_2} + \frac{\partial v_2}{\partial x_2}\right),
\end{aligned}
\tag{6}
$$

where

$$
\begin{aligned}
&Q_{111} = \frac{E_{111}}{1-\nu_{112}\nu_{121}},\ Q_{112} = \frac{E_{111}\nu_{121}}{1-\nu_{112}\nu_{121}},\ Q_{122} = \frac{E_{122}}{1-\nu_{112}\nu_{121}},\\
&Q_{211} = \frac{E_{211}}{1-\nu_{212}\nu_{221}},\ Q_{212} = \frac{E_{211}\nu_{221}}{1-\nu_{212}\nu_{221}},\ Q_{222} = \frac{E_{222}}{1-\nu_{212}\nu_{221}}.
\end{aligned}
\tag{7}
$$

Assuming both the plates have the same height and in-plane dimensions, the kinetic energy of the carbon nanotubes reinforced double plates with elastic layer then can be written as follows

$$
K = \frac{1}{2}\int_{-h/2}^{h/2}\int_0^a\int_0^b \left\{
\begin{aligned}
&\rho_1(z)\left[\begin{aligned}&\left(\frac{\partial u_1}{\partial t}\right)^2 + \left(\frac{\partial v_1}{\partial t}\right)^2 + \left(\frac{\partial w_1}{\partial t}\right)^2 + z^2\left(\frac{\partial^2 w_1}{\partial x\partial t}\right)^2\\ &-2z\frac{\partial u_1}{\partial t}\frac{\partial^2 w_1}{\partial x\partial t} + z^2\left(\frac{\partial^2 w_1}{\partial y\partial t}\right)^2 - 2z\frac{\partial v_1}{\partial t}\frac{\partial^2 w_1}{\partial y\partial t}\end{aligned}\right]\\
&+\rho_2(z)\left[\begin{aligned}&\left(\frac{\partial u_2}{\partial t}\right)^2 + \left(\frac{\partial v_2}{\partial t}\right)^2 + \left(\frac{\partial w_2}{\partial t}\right)^2 + z^2\left(\frac{\partial^2 w_2}{\partial x\partial t}\right)^2\\ &-2z\frac{\partial u_2}{\partial t}\frac{\partial^2 w_2}{\partial x\partial t} + z^2\left(\frac{\partial^2 w_2}{\partial y\partial t}\right)^2 - 2z\frac{\partial v_2}{\partial t}\frac{\partial^2 w_2}{\partial y\partial t}\end{aligned}\right]
\end{aligned}
\right\} dxdydz.
\tag{8}
$$

The strain energy of the carbon nanotubes reinforced double plates with elastic layer can be expressed as

$$U=\frac{1}{2}\int_{-h/2}^{h/2}\int_{0}^{a}\int_{0}^{b}\left\{\begin{aligned}&\left[Q_{111}\left(\frac{\partial u_1}{\partial x}-z\frac{\partial^2 w_1}{\partial x^2}\right)+Q_{112}\left(\frac{\partial v_1}{\partial y}-z\frac{\partial^2 w_1}{\partial y^2}\right)\right]\left(\frac{\partial u_1}{\partial x}-z\frac{\partial^2 w_1}{\partial x^2}\right)\\&+\left[Q_{122}\left(\frac{\partial v_1}{\partial y}-z\frac{\partial^2 w_1}{\partial y^2}\right)+Q_{112}\left(\frac{\partial u_1}{\partial x}-z\frac{\partial^2 w_1}{\partial x^2}\right)\right]\left(\frac{\partial v_1}{\partial y}-z\frac{\partial^2 w_1}{\partial y^2}\right)\\&+G_{112}\left(\frac{\partial u_1}{\partial y}-2z\frac{\partial^2 w_1}{\partial x\partial y}+\frac{\partial v_1}{\partial x}\right)^2\\&+\left[Q_{211}\left(\frac{\partial u_2}{\partial x}-z\frac{\partial^2 w_2}{\partial x^2}\right)+Q_{212}\left(\frac{\partial v_2}{\partial y}-z\frac{\partial^2 w_2}{\partial y^2}\right)\right]\left(\frac{\partial u_2}{\partial x}-z\frac{\partial^2 w_2}{\partial x^2}\right)\\&+\left[Q_{222}\left(\frac{\partial v_2}{\partial y}-z\frac{\partial^2 w_2}{\partial y^2}\right)+Q_{212}\left(\frac{\partial u_2}{\partial x}-z\frac{\partial^2 w_2}{\partial x^2}\right)\right]\left(\frac{\partial v_2}{\partial y}-z\frac{\partial^2 w_2}{\partial y^2}\right)\\&+G_{212}\left(\frac{\partial u_2}{\partial y}-2z\frac{\partial^2 w_2}{\partial x\partial y}+\frac{\partial v_2}{\partial x}\right)^2\end{aligned}\right\}dydxdz$$
$$+\frac{1}{2}\int_{0}^{a}\int_{0}^{b}k\left(w_1-w_2\right)^2dydx. \tag{9}$$

By employing the Hamilton principle and utilising Eqs. (8) and (9), the following equations are derived to describe the interconnected in-plane and transverse motions

$$\begin{aligned}&I_{11}\frac{\partial^2 u_1}{\partial t^2}-I_{12}\frac{\partial^3 w_1}{\partial x\partial t^2}-\frac{\partial}{\partial x}\left(A_{11}\frac{\partial u_1}{\partial x}+B_{11}\frac{\partial v_1}{\partial y}-A_{12}\frac{\partial^2 w_1}{\partial x^2}-B_{12}\frac{\partial^2 w_1}{\partial y^2}\right)\\&-\frac{\partial}{\partial y}\left(D_{11}\left(\frac{\partial u_1}{\partial y}+\frac{\partial v_1}{\partial x}\right)-2D_{12}\frac{\partial^2 w_1}{\partial x\partial y}\right)=0,\\&I_{21}\frac{\partial^2 u_2}{\partial t^2}-I_{22}\frac{\partial^3 w_2}{\partial x\partial t^2}-\frac{\partial}{\partial x}\left(A_{21}\frac{\partial u_2}{\partial x}+B_{21}\frac{\partial v_2}{\partial y}-A_{22}\frac{\partial^2 w_2}{\partial x^2}-B_{22}\frac{\partial^2 w_2}{\partial y^2}\right)\\&-\frac{\partial}{\partial y}\left(D_{21}\left(\frac{\partial u_2}{\partial y}+\frac{\partial v_2}{\partial x}\right)-2D_{22}\frac{\partial^2 w_2}{\partial x\partial y}\right)=0,\end{aligned} \tag{10}$$

$$\begin{aligned}&I_{11}\frac{\partial^2 v_1}{\partial t^2}-I_{12}\frac{\partial^3 w_1}{\partial y\partial t^2}-\frac{\partial}{\partial x}\left(D_{11}\left(\frac{\partial u_1}{\partial y}+\frac{\partial v_1}{\partial x}\right)-2D_{12}\frac{\partial^2 w_1}{\partial x\partial y}\right)\\&-\frac{\partial}{\partial y}\left(C_{11}\frac{\partial v_1}{\partial y}+B_{11}\frac{\partial u_1}{\partial x}-C_{12}\frac{\partial^2 w_1}{\partial y^2}-B_{12}\frac{\partial^2 w_1}{\partial x^2}\right)=0,\\&I_{21}\frac{\partial^2 v_2}{\partial t^2}-I_{22}\frac{\partial^3 w_2}{\partial y\partial t^2}-\frac{\partial}{\partial x}\left(D_{21}\left(\frac{\partial u_2}{\partial y}+\frac{\partial v_2}{\partial x}\right)-2D_{22}\frac{\partial^2 w_2}{\partial x\partial y}\right)\\&-\frac{\partial}{\partial y}\left(C_{21}\frac{\partial v_2}{\partial y}+B_{21}\frac{\partial u_2}{\partial x}-C_{22}\frac{\partial^2 w_2}{\partial y^2}-B_{22}\frac{\partial^2 w_2}{\partial x^2}\right)=0,\end{aligned} \tag{11}$$

$$
\begin{aligned}
&I_{11}\frac{\partial^2 w_1}{\partial t^2}+I_{12}\left(\frac{\partial^3 u_1}{\partial x\partial t^2}+\frac{\partial^3 v_1}{\partial y\partial t^2}\right)-I_{13}\left(\frac{\partial^4 w_1}{\partial x^2\partial t^2}+\frac{\partial^4 w_1}{\partial y^2\partial t^2}\right)+k\left(w_1-w_2\right)\\
&-\frac{\partial}{\partial x^2}\left(A_{12}\frac{\partial u_1}{\partial x}+B_{12}\frac{\partial v_1}{\partial y}-A_{13}\frac{\partial^2 w_1}{\partial x^2}-B_{13}\frac{\partial^2 w_1}{\partial y^2}\right)\\
&-\frac{\partial}{\partial y^2}\left(C_{12}\frac{\partial v_1}{\partial y}+B_{12}\frac{\partial u_1}{\partial x}-C_{13}\frac{\partial^2 w_1}{\partial y^2}-B_{13}\frac{\partial^2 w_1}{\partial x^2}\right)\\
&-\frac{\partial^2}{\partial x\partial y}\left(2D_{12}\left(\frac{\partial u_1}{\partial y}+\frac{\partial v_1}{\partial x}\right)-4D_{13}\frac{\partial^2 w_1}{\partial x\partial y}\right)=0,\\
&I_{21}\frac{\partial^2 w_2}{\partial t^2}+I_{22}\left(\frac{\partial^3 u_2}{\partial x\partial t^2}+\frac{\partial^3 v_2}{\partial y\partial t^2}\right)-I_{23}\left(\frac{\partial^4 w_2}{\partial x^2\partial t^2}+\frac{\partial^4 w_2}{\partial y^2\partial t^2}\right)-k\left(w_1-w_2\right)\\
&-\frac{\partial}{\partial x^2}\left(A_{22}\frac{\partial u_2}{\partial x}+B_{22}\frac{\partial v_2}{\partial y}-A_{23}\frac{\partial^2 w_2}{\partial x^2}-B_{23}\frac{\partial^2 w_2}{\partial y^2}\right)\\
&-\frac{\partial}{\partial y^2}\left(C_{22}\frac{\partial v_2}{\partial y}+B_{22}\frac{\partial u_2}{\partial x}-C_{23}\frac{\partial^2 w_2}{\partial y^2}-B_{23}\frac{\partial^2 w_2}{\partial x^2}\right)\\
&-\frac{\partial^2}{\partial x\partial y}\left(2D_{22}\left(\frac{\partial u_2}{\partial y}+\frac{\partial v_2}{\partial x}\right)-4D_{23}\frac{\partial^2 w_2}{\partial x\partial y}\right)=0.
\end{aligned}
\tag{12}
$$

The following area moments of inertia about the *z* axis, and the stiffness terms can be expressed as

$$
\left\{I_{i1}\quad I_{i2}\quad I_{i3}\right\}=\int_{-h/2}^{h/2}\rho_i\left(z\right)\left\{1\quad z\quad z^2\right\}dz,
\tag{13}
$$

$$
\begin{aligned}
\left\{A_{i1}\quad A_{i2}\quad A_{i3}\right\}&=\int_{-h/2}^{h/2}\frac{E_{i11}\left(z\right)}{1-\nu_{i12}\left(z\right)\nu_{i21}\left(z\right)}\left\{1\quad z\quad z^2\right\}dz,\\
\left\{B_{i1}\quad B_{i2}\quad B_{i3}\right\}&=\int_{-h/2}^{h/2}\frac{\nu_{i21}\left(z\right)E_{i11}\left(z\right)}{1-\nu_{i12}\left(z\right)\nu_{i21}\left(z\right)}\left\{1\quad z\quad z^2\right\}dz,\\
\left\{C_{i1}\quad C_{i2}\quad C_{i3}\right\}&=\int_{-h/2}^{h/2}\frac{E_{i22}\left(z\right)}{1-\nu_{i12}\left(z\right)\nu_{i21}\left(z\right)}\left\{1\quad z\quad z^2\right\}dz,\\
\left\{D_{i1}\quad D_{i2}\quad D_{i3}\right\}&=\int_{-h/2}^{h/2}G_{i12}\left(z\right)\left\{1\quad z\quad z^2\right\}dz,
\end{aligned}
\tag{14}
$$

where i = 1, 2.

Nondimensionalising Eqs. (10), (11) and (12) using

$$
\begin{aligned}
&x^* = \frac{x}{a},\ y^* = \frac{y}{b},\ u_i^* = \frac{u_i}{h},\ v_i^* = \frac{v_i}{h},\ w_i^* = \frac{w_i}{h},\ \phi = \frac{b}{a},\ \gamma = \frac{b}{h},\\
&t^* = t\sqrt{\frac{A_{13,m}}{I_{11,m}b^4}},\ k^* = k\frac{b^4}{A_{13,m}},\ D_{i1}^* = \frac{D_{i1}h^2}{A_{13,m}},\ D_{i2}^* = \frac{D_{i2}h}{A_{13,m}},\ D_{i3}^* = \frac{D_{i3}}{A_{13,m}},\\
&I_{i1}^* = \frac{I_{i1}}{I_{11,m}},\ I_{i2}^* = \frac{I_{i2}}{I_{11,m}h},\ I_{i3}^* = \frac{I_{i3}}{I_{11,m}h^2},\ A_{i1}^* = \frac{A_{i1}h^2}{A_{13,m}},\ A_{i2}^* = \frac{A_{i2}h}{A_{13,m}},\ A_{i3}^* = \frac{A_{i3}}{A_{13,m}},\\
&B_{i1}^* = \frac{B_{i1}h^2}{A_{13,m}},\ B_{i2}^* = \frac{B_{i2}h}{A_{13,m}},\ B_{i3}^* = \frac{B_{i3}}{A_{13,m}},\ C_{i1}^* = \frac{C_{i1}h^2}{A_{13,m}},\ C_{i2}^* = \frac{C_{i2}h}{A_{13,m}},\ C_{i3}^* = \frac{C_{i3}}{A_{13,m}},
\end{aligned}
\tag{15}
$$

results in

$$
\begin{aligned}
&I_{11}\frac{\partial^2 u_1}{\partial t^2} - I_{12}\frac{\phi}{\gamma}\frac{\partial^3 w_1}{\partial x \partial t^2} - \frac{\partial}{\partial x}\left(\phi^2\gamma^2 A_{11}\frac{\partial u_1}{\partial x} + \phi\gamma^2 B_{11}\frac{\partial v_1}{\partial y} - \phi^3\gamma A_{12}\frac{\partial^2 w_1}{\partial x^2} - \phi\gamma B_{12}\frac{\partial^2 w_1}{\partial y^2}\right)\\
&-\frac{\partial}{\partial y}\left(D_{11}\left(\gamma^2\frac{\partial u_1}{\partial y} + \phi\gamma^2\frac{\partial v_1}{\partial x}\right) - 2D_{12}\phi\gamma\frac{\partial^2 w_1}{\partial x \partial y}\right) = 0,\\
&I_{21}\frac{\partial^2 u_2}{\partial t^2} - I_{22}\frac{\phi}{\gamma}\frac{\partial^3 w_2}{\partial x \partial t^2} - \frac{\partial}{\partial x}\left(\phi^2\gamma^2 A_{21}\frac{\partial u_2}{\partial x} + \phi\gamma^2 B_{21}\frac{\partial v_2}{\partial y} - \phi^3\gamma A_{22}\frac{\partial^2 w_2}{\partial x^2} - \phi\gamma B_{22}\frac{\partial^2 w_2}{\partial y^2}\right)\\
&-\frac{\partial}{\partial y}\left(D_{21}\left(\gamma^2\frac{\partial u_2}{\partial y} + \phi\gamma^2\frac{\partial v_2}{\partial x}\right) - 2D_{22}\phi\gamma\frac{\partial^2 w_2}{\partial x \partial y}\right) = 0,
\end{aligned}
\tag{16}
$$

$$
\begin{aligned}
&I_{11}\frac{\partial^2 v_1}{\partial t^2} - I_{12}\frac{1}{\gamma}\frac{\partial^3 w_1}{\partial y \partial t^2} - \frac{\partial}{\partial x}\left(D_{11}\left(\phi\gamma^2\frac{\partial u_1}{\partial y} + \phi^2\gamma^2\frac{\partial v_1}{\partial x}\right) - 2D_{12}\phi^2\gamma\frac{\partial^2 w_1}{\partial x \partial y}\right)\\
&-\frac{\partial}{\partial y}\left(C_{11}\gamma^2\frac{\partial v_1}{\partial y} + B_{11}\phi\gamma^2\frac{\partial u_1}{\partial x} - C_{12}\gamma\frac{\partial^2 w_1}{\partial y^2} - B_{12}\phi^2\gamma\frac{\partial^2 w_1}{\partial x^2}\right) = 0,\\
&I_{21}\frac{\partial^2 v_2}{\partial t^2} - I_{22}\frac{1}{\gamma}\frac{\partial^3 w_2}{\partial y \partial t^2} - \frac{\partial}{\partial x}\left(D_{21}\left(\phi\gamma^2\frac{\partial u_2}{\partial y} + \phi^2\gamma^2\frac{\partial v_2}{\partial x}\right) - 2D_{22}\phi^2\gamma\frac{\partial^2 w_2}{\partial x \partial y}\right)\\
&-\frac{\partial}{\partial y}\left(C_{21}\gamma^2\frac{\partial v_2}{\partial y} + B_{21}\phi\gamma^2\frac{\partial u_2}{\partial x} - C_{22}\gamma\frac{\partial^2 w_2}{\partial y^2} - B_{22}\phi^2\gamma\frac{\partial^2 w_2}{\partial x^2}\right) = 0,
\end{aligned}
\tag{17}
$$

$$
\begin{aligned}
&I_{11}\frac{\partial^2 w_1}{\partial t^2}+I_{12}\left(\frac{\phi}{\gamma}\frac{\partial^3 u_1}{\partial x\partial t^2}+\frac{1}{\gamma}\frac{\partial^3 v_1}{\partial y\partial t^2}\right)-I_{13}\left(\frac{\phi^2}{\gamma^2}\frac{\partial^4 w_1}{\partial x^2\partial t^2}+\frac{1}{\gamma^2}\frac{\partial^4 w_1}{\partial y^2\partial t^2}\right)+k\left(w_1-w_2\right)\\
&-\frac{\partial}{\partial x^2}\left(A_{12}\phi^3\gamma\frac{\partial u_1}{\partial x}+B_{12}\phi^2\gamma\frac{\partial v_1}{\partial y}-A_{13}\phi^4\frac{\partial^2 w_1}{\partial x^2}-B_{13}\phi^2\frac{\partial^2 w_1}{\partial y^2}\right)\\
&-\frac{\partial}{\partial y^2}\left(C_{12}\gamma\frac{\partial v_1}{\partial y}+B_{12}\phi\gamma\frac{\partial u_1}{\partial x}-C_{13}\frac{\partial^2 w_1}{\partial y^2}-B_{13}\phi^2\frac{\partial^2 w_1}{\partial x^2}\right)\\
&-\frac{\partial^2}{\partial x\partial y}\left(2D_{12}\left(\phi\gamma\frac{\partial u_1}{\partial y}+\phi^2\gamma\frac{\partial v_1}{\partial x}\right)-4D_{13}\phi^2\frac{\partial^2 w_1}{\partial x\partial y}\right)=0,\\
&I_{21}\frac{\partial^2 w}{\partial t^2}+I_{22}\left(\frac{\phi}{\gamma}\frac{\partial^3 u_2}{\partial x\partial t^2}+\frac{1}{\gamma}\frac{\partial^3 v_2}{\partial y\partial t^2}\right)-I_{23}\left(\frac{\phi^2}{\gamma^2}\frac{\partial^4 w_2}{\partial x^2\partial t^2}+\frac{1}{\gamma^2}\frac{\partial^4 w_2}{\partial y^2\partial t^2}\right)-k\left(w_1-w_2\right)\\
&-\frac{\partial}{\partial x^2}\left(A_{22}\phi^3\gamma\frac{\partial u_2}{\partial x}+B_{22}\phi^2\gamma\frac{\partial v_2}{\partial y}-A_{23}\phi^4\frac{\partial^2 w_2}{\partial x^2}-B_{23}\phi^2\frac{\partial^2 w_2}{\partial y^2}\right)\\
&-\frac{\partial}{\partial y^2}\left(C_{22}\gamma\frac{\partial v_2}{\partial y}+B_{22}\phi\gamma\frac{\partial u_2}{\partial x}-C_{23}\frac{\partial^2 w_2}{\partial y^2}-B_{23}\phi^2\frac{\partial^2 w_2}{\partial x^2}\right)\\
&-\frac{\partial^2}{\partial x\partial y}\left(2D_{22}\left(\phi\gamma\frac{\partial u_2}{\partial y}+\phi^2\gamma\frac{\partial v_2}{\partial x}\right)-4D_{23}\phi^2\frac{\partial^2 w_2}{\partial x\partial y}\right)=0.
\end{aligned}
\tag{18}
$$

2.3. Solution technique

The discretisation technique of two-spatial-variable modal decomposition is utilised to solve the system of six coupled Eqs. (16), (17) and (18). The in-plane and transverse motions of the functionally graded carbon nanotubes reinforced rectangular double plates with simply supported boundary conditions are expanded in the following manner:

$$
\begin{aligned}
u_1&=\sum_{q=1}^{M}\sum_{r=1}^{N}u_{1q,r}\left(t\right)\sin\left(\frac{q\pi x}{a}\right)\sin\left(\frac{r\pi y}{b}\right),\\
u_2&=\sum_{q=1}^{M}\sum_{r=1}^{N}u_{2q,r}\left(t\right)\sin\left(\frac{q\pi x}{a}\right)\sin\left(\frac{r\pi y}{b}\right),\\
v_1&=\sum_{q=1}^{M}\sum_{r=1}^{N}v_{1q,r}\left(t\right)\sin\left(\frac{q\pi x}{a}\right)\sin\left(\frac{r\pi y}{b}\right),\\
v_2&=\sum_{q=1}^{M}\sum_{r=1}^{N}v_{2q,r}\left(t\right)\sin\left(\frac{q\pi x}{a}\right)\sin\left(\frac{r\pi y}{b}\right),\\
w_1&=\sum_{q=1}^{M}\sum_{r=1}^{N}w_{1q,r}\left(t\right)\sin\left(\frac{q\pi x}{a}\right)\sin\left(\frac{r\pi y}{b}\right),\\
w_2&=\sum_{q=1}^{M}\sum_{r=1}^{N}w_{2q,r}\left(t\right)\sin\left(\frac{q\pi x}{a}\right)\sin\left(\frac{r\pi y}{b}\right),
\end{aligned}
\tag{19}
$$

where M and N represent the respective numbers of half-waves in the x and y directions, whereas $u_{iq,r}(t)$, $v_{iq,r}(t)$, and $w_{iq,r}(t)$ denote the generalised coordinates that are numerically determined.

By applying the modal decomposition and substituting Eq. (19) into Eqs. (16), (17) and (18), and obtaining the inertial and stiffness matrices, the natural frequencies of the simply supported functionally graded carbon nanotubes reinforced rectangular double plates can be determined.

3. Verifications of equations of motion and solution technique

To ensure the accuracy and reliability of the equations and solution technique proposed above, this section outlines the verifications procedures and present the corresponding results.

3.1. Equation verification

To verify the mathematical equations developed, a *non*-carbon-nanotube reinforced (isotropic) double plates with elastic layer is considered, where

$$
\begin{aligned}
&A_{i1} = C_{i1},\ A_{i3} = C_{i3},\\
&I_{i2} = A_{i2} = B_{i2} = C_{i2} = D_{i2} = 0,\\
&4D_{i3} + 2B_{i3} = 2A_{i3},\\
&A_{i1} = \frac{E_{i11}h}{\left(1-v_i^2\right)},\ A_{i3} = \frac{E_{i11}h^3}{12\left(1-v_i^2\right)},\\
&I_{i1} = \rho_i h,\ I_{i3} = \frac{\rho_i h^3}{12}.
\end{aligned}
\tag{20}
$$

Ignoring in-plane motions, the equations are then simplified to

$$
\begin{aligned}
&\rho_1 h\frac{\partial^2 w_1}{\partial t^2} - \frac{\rho_1 h^3}{12}\left(\frac{\partial^4 w_1}{\partial x^2\partial t^2} + \frac{\partial^4 w_1}{\partial y^2\partial t^2}\right) + \frac{E_{111}h^3}{12\left(1-v_1^2\right)}\left(\frac{\partial^4 w_1}{\partial x^4} + \frac{\partial^4 w_1}{\partial y^4} + 2\frac{\partial^4 w_1}{\partial x^2\partial y^2}\right)\\
&+k\left(w_1 - w_2\right) = 0,\\
&\rho_2 h\frac{\partial^2 w_2}{\partial t^2} - \frac{\rho_2 h^3}{12}\left(\frac{\partial^4 w_2}{\partial x^2\partial t^2} + \frac{\partial^4 w_2}{\partial y^2\partial t^2}\right) + \frac{E_{211}h^3}{12\left(1-v_2^2\right)}\left(\frac{\partial^4 w_2}{\partial x^4} + \frac{\partial^4 w_2}{\partial y^4} + 2\frac{\partial^4 w_2}{\partial x^2\partial y^2}\right)\\
&-k\left(w_1 - w_2\right) = 0.
\end{aligned}
\tag{21}
$$

The equations of motion obtained were compared to the equations found in the existing literature (Ref. [59]) for a double plates model, and they were found to be consistent.

Further simplifying the kinetic energy term by excluding the rotational term in Eq. (8), Eq. (21) becomes

$$\begin{aligned}
&\rho_1 h\frac{\partial^2 w_1}{\partial t^2}+\frac{E_{111}h^3}{12\left(1-v_1^2\right)}\left(\frac{\partial^4 w_1}{\partial x^4}+\frac{\partial^4 w_1}{\partial y^4}+2\frac{\partial^4 w_1}{\partial x^2\partial y^2}\right)+k\left(w_1-w_2\right)=0,\\
&\rho_2 h\frac{\partial^2 w_2}{\partial t^2}+\frac{E_{211}h^3}{12\left(1-v_2^2\right)}\left(\frac{\partial^4 w_2}{\partial x^4}+\frac{\partial^4 w_2}{\partial y^4}+2\frac{\partial^4 w_2}{\partial x^2\partial y^2}\right)-k\left(w_1-w_2\right)=0.
\end{aligned} \tag{22}$$

Eq. (22) was found to be the same as those of Ref. [55].

3.2. Solution technique verification

(a) *Existing literature*

The solutions technique is verified by comparing the natural frequency of the two simplified versions of the system by solving the equations of motion using the methodology of the current study with numerical results available in the literature.

The first model employed is a functionally graded carbon nanotubes reinforced *single* plate with simply supported boundary conditions, where h/b = 0.02. The first three natural frequencies obtained from the current study and Ref. [66] for the different carbon nanotubes volume fractions, and functionally graded patterns are tabulated in Table 1(a). A very good level of agreement was achieved.

The second model used is a simply supported *non*-carbon-nanotube reinforced (isotropic) double plates with an elastic layer. The dimensional natural frequencies (rad/s) of the system obtained using the current methodology and in Ref. [55] are tabulated in Table 1(b). A very good level of agreement was also achieved.

(b) *FEM modelling*

The free vibrational behaviour of a simply supported *non*-carbon-nanotube reinforced (isotropic) double square plates with elastic layer was investigated using the FEM, specifically ANSYS® (version 2022 R2, ANSYS Inc., Canonsburg, PA, USA). The elastic layer is modelled by using an elastic material with an equivalent dimensional stiffness coefficient, k, of 1 x 10^6 N/m^3. The appropriate mesh size to ensure convergence of the natural frequencies solutions is selected. The square plates have dimensions of $a = b$ = 1 m and h = 0.01 m, and material properties of ρ = 7850 kg/m^3, E = 2.1 GPa, and v = 0.3. The natural frequencies of the

non-carbon-nanotube reinforced (isotropic) double square plates in Hz obtained using the FEM and the modal decomposition method are tabulated in Table 1(c) where excellent agreement was noted.

The corresponding first and second series mode shapes of each mode obtained from the MDM are shown in Figs. 2 and 3. The mode shapes obtained from the FEM are shown in Figs. 4 and 5 instead for comparison. Each mode compromises of two series, where in the first series, the double plates vibrate in an independent manner. The higher modes consist of higher numbers of nodes and exemplify more complex vibrational patterns. The m in $\omega_{m,qr}$ denotes the series number.

4. Results

To demonstrate the dynamics of the functionally graded carbon nanotubes reinforced double plates, for the numerical section, the material properties and plates dimensions used are: ρ_{CNT} = 1400 kg/m^3, E_{11CNT} = 5.6466 TPa, E_{22CNT} = 7.08 TPa, G_{12CNT} = 1.9445 TPa, v_{12CNT} = 0.175, ρ_m = 1150 kg/m^3, E_m = 2.1 GPa, v_m = 0.34 [67], a = b = 1 m, and h/b = 0.02. Firstly, to ensure the convergence of the solutions, increasing the number of modes used for the solving process, the lateral and axial motion natural frequencies of a FG-X carbon nanotubes reinforced square double plates are plotted in Fig. 6. As anticipated, the natural frequency of both the in-plane directions converges as the number of modes increases; 42 modes were selected for the numerical calculations.

In order to investigate the impact of the in-plane dimensions of the UD carbon nanotubes reinforced rectangular double plates on the transverse-motion natural frequency, aspect ratios (b/a) of 0.25 to 4 were considered. This involved varying the value of b in the range of 0.25 m to 4 m, while keeping a (1 m) and h (0.005 m) constant. Setting the dimensional stiffness coefficient, k, to 10 x 10^6 N/m^3, the first series dimensional transverse-motion natural frequencies (rad/s) for the four different volume fractions of the carbon nanotubes (including $V_{CNT}^{*} = 0$) are plotted in Fig. 7. Generally, the transverse-motion natural frequency of all the modes decreases as the aspect ratio increases, for all the cases. However, the rate of decrease decreases as the aspect ratio increases. It is noted that the rate of decrease of natural frequencies varies for different carbon nanotubes volume fractions. Most modes provide a higher natural frequency as carbon nanotubes volume fractions increases, except for mode 1,12, where it only

happens after b/a exceeds approximately 0.45. Initially (b/a = 0.25) for mode 1,12, V_{CNT}^{*} of 0.17 provides the highest natural frequency, followed by 0 (non-reinforced), 0.14 and 0.11. Due to the aspect ratio, mode 1,12 also possesses higher natural frequency than mode 1,21, for all systems, initially. The natural frequency of mode 1,21 eventually overtakes mode 1,12, precisely when b/a = 1 for non-reinforced double plates. This also means the transverse-motion natural frequency of mode 1,12 declines in a larger rate as the aspect ratio increases when compared with mode 1,21.

In Fig. 8, the plotted dimensional transverse-motion natural frequencies for the second series are depicted. Largely following the similar trends of the first series, as the aspect ratio increases, the double plates transverse-motion natural frequency of all the modes decreases. The second series transverse-motion natural frequencies are always higher than the first series due to the effect of the elastic layer. This elastic layer effect is more pronounced for the non-reinforced systems, which led to larger differences in natural frequencies between the two series when compared with the reinforced systems. Additionally, increasing the value of carbon nanotubes volume fractions, does not result in higher values of $\omega_{2,11}$ and $\omega_{2,12}$ for all aspect ratios. For mode 2,11, the natural frequency of the non-reinforced system is always the highest. As the aspect ratio increases beyond 0.4, the higher the carbon nanotubes volume fractions, the lower the natural frequency of the system, demonstrating the effect of the elastic layer. The same applies for mode 2,12 as the aspect ratio increases beyond 0.7. Overall, the double plates system has shown larger transverse-motion natural frequencies changes to both the series of natural frequencies initially. The first series also shown larger changes to natural frequencies than the second series as the aspect ratio changes. For all the double plates systems, the transverse-motion natural frequency is lowest when the aspect ratio is 4.

To further evaluate the effect of the aspect ratio on the system, the fundamental (mode 11) lateral and axial-motion natural frequencies are plotted in Fig. 9. Since the elastic layer is assumed to only be acting on the transverse direction, there is only one series of natural frequency for both the directions. For both the motions, the natural frequency decreases as the aspect ratio increases, for all the carbon nanotubes volume fractions. As the aspect ratio increases, there is a decline in the rate of decrease. For the lateral motion, the natural frequency does not differ too much for the first three cases of carbon nanotubes volume fractions when compared with V_{CNT}^{*} of 0.17. Initially, a carbon nanotubes volume fraction of 0.17 has the highest lateral-motion natural frequency, followed by 0, and 0.14, with 0.11 being the lowest.

The axial motion possesses higher natural frequencies as the carbon nanotubes volume fraction increases.

To examine how the thicknesses of the square plates, reinforced with UD carbon nanotubes, affects its out-of-plane natural frequencies, the ratio of the plate length to height (b/h) is varied within the range of 50 to 100. Different carbon nanotubes volume fractions are considered while keeping $a = b = 1.5$ m and $k = 6 \times 10^6$ N/m^3. The first series dimensional transverse-motion natural frequencies (rad/s) are plotted in Fig. 10. All natural frequencies follow a similar trend, where an increase in thickness (from the right to the left of the graph) leads to an increase in the values of $\omega_{1,11}$, $\omega_{1,12}$, $\omega_{1,21}$, and $\omega_{1,22}$. This is expected as thicker plates are stiffer than thin plates. The rate of increase becomes higher as the thickness of the plates increases. The transverse-motion natural frequencies are also more sensitive towards thickness changes when the plates are reinforced by carbon nanotubes. It is also observed that the difference of transverse-motion natural frequencies between different carbon nanotubes volume fractions increase as the thickness of the double plates increases.

Figure 11 displays the plotted dimensional transverse-motion natural frequencies for the second series as the thicknesses of the plates is varied. With higher values of natural frequencies, the second series natural frequencies generally exhibit different behaviour from the first series counterpart. The values of $\omega_{2,11}$ generally decreases as the plates' thicknesses increases, except for the case of $V_{CNT}^{*} = 0.17$, where a slight increasing trend is noted when the thicknesses increase beyond $b/h = 52$. It appears the effect of elastic layer is more prominent when the plates are thinner. The values of $\omega_{2,12}$ for all the reinforced systems follow a decreasing trend initially as plates' thicknesses increase till they reach a minimum point; then follow an increasing trend as the thicknesses increase further. The non-reinforced system exhibits a decreasing trend for both modes. However, for modes 2,21 and 2,22, the natural frequency of the reinforced systems demonstrates an increasing behaviour as the thicknesses increase. On the other hand, the non-reinforced system natural frequency decreases as plates' thicknesses increase for mode 2,21 for all thicknesses but increases after it reaches a minimum point for mode 2,22. Generally, the thinner plates systems have smaller natural frequencies differences between the different carbon nanotubes volume fractions when compared with thicker plates.

In order to investigate the impact of different elastic layer stiffness and carbon nanotubes volume fractions, Fig. 12 showcases the plotted second series transverse-motion natural frequencies of a simply supported UD carbon nanotubes reinforced square double plates. The

dimensionless elastic layer stiffness, k^*, is varied in a range of 0 – 30000. It is noted changing the stiffness of the elastic layer does not affect the first series natural frequencies. The introduction of the elastic layer leads to an increase in all the plotted natural frequencies. The effect is more evident at the start of the introduction of elastic layer for $\omega_{2,11}$ and $\omega_{2,12}$, with a larger increase in natural frequencies is observed, especially for the reinforced systems. The effects of carbon nanotubes reinforcement become less notable with the differences of natural frequencies between different carbon nanotubes volume fractions become smaller as the stiffness of the elastic layer increases, especially for $\omega_{2,11}$ and $\omega_{2,12}$.

To examine and understand the effects of functionally graded patterns of the carbon nanotubes reinforced double plates, the natural frequencies of systems reinforced by carbon nanotubes with FG-O and FG-X patterns are plotted in Figs. 13 and 14, respectively, with varying elastic layer stiffness. Following a general increasing trend with the introduction of elastic layer, the FG-X pattern possess the largest natural frequencies for all cases. The FG-O pattern has the lowest natural frequencies compared to the two other functionally graded patterns.

5. Conclusions

The purpose of this study was to examine the free vibrations of simply supported functionally graded carbon nanotubes reinforced double plates connected by an elastic layer. Three carbon nanotubes functionally graded patterns were considered in this study: uniformly distributed, FG-O, and FG-X. The coupled equations of motion are developed using the Kirchhoff plate theory and the Hamilton principle. The equations were then solved using the modal decomposition method and verified by comparing them to simplified models from existing studies. The numerical results for simplified configurations obtained from the finite element method (FEM) and existing studies were compared with the results obtained using the proposed solution methodology. Good agreement was noted for both verifications. The research shown that increasing plates' aspect ratios cause the first and second series transverse-motion natural frequencies to decrease. A similar trend can be observed for the lateral and axial-motion natural frequencies. The effect of reinforcement of carbon nanotubes is also less notable as the plates become thinner. The introduction of elastic layer increases the second series transverse-motion natural frequencies. The FG-X carbon nanotubes pattern always

possesses the highest transverse-motion natural frequency. The suitable CNT distribution is subjected to the design requirements of the double plates.

Acknowledgement

We express our gratitude for the support provided by The University of Adelaide through the Adelaide Graduate Research Scholarship.

References

[1] Soedel W. Vibrations of shells and plates: CRC Press; 2004.
[2] Kanok-Nukulchai W. Finite element formulation for plate stability analysis. Analysis and Design of Plated Structures: Elsevier; 2022. 109-32.
[3] Fotiu P, Irschik H, Ziegler F. Modal analysis of elastic-plastic plate vibrations by integral equations. Engineering Analysis with Boundary Elements 1994;14(1): 81-97.
[4] Chakraverty S. Vibration of plates: CRC Press; 2008.
[5] Barati MR, Shahverdi H. Assessment of nonlinear vibrations of thin plates undergoing large deflection and moderate rotation using Jacobi elliptic functions. Mechanics Based Design of Structures and Machines 2023;51(8): 4255-71.
[6] Karimi A, Alahdadi S, Ghayour M. Dynamic analysis of a rectangular plate subjected to a mass moving with variable velocity on a predefined path or an arbitrary one. Thin-Walled Structures 2021;160: 107340.
[7] Zhang J, Du X, Chen Y, Guo X, Li L, Zhang D. Free vibration analysis of a rotating skew plate by using the absolute nodal coordinate formulation. Thin-Walled Structures 2023;188: 110840.
[8] Foyouzat M. Separation/recontact investigation of a travelling oscillator over a plate with inclusion of surface roughness. Thin-Walled Structures 2023;183: 110373.
[9] Kubiak T, Borkowski L, Perlikowski P. Some aspects of dynamic buckling and dynamic response of thin plate under in-plane compression. Thin-Walled Structures 2023;182: 110294.
[10] Shubhra QT, Alam AM, Quaiyyum MA. Mechanical properties of polypropylene composites: A review. Journal of Thermoplastic Composite Materials 2013;26(3): 362-91.
[11] Ghosh S, Haldar S. Cutout effects on the dynamic analysis of laminated composite plates resting on two-parameter elastic foundation. Mechanics Based Design of Structures and Machines 2023: 1-32.
[12] Nachiappan Sevugan A, Murugan H, Ramamoorthy M, Rajamohan V. Modeling and analysis of tapered composite beams with piezoelectric energy harvester: Numerical and experimental investigations. Mechanics Based Design of Structures and Machines 2023: 1-20.
[13] Yang W, Yan G, Wu W, Zou X, Sun Y, He S. Wave dispersion analysis of natural fiber-strengthened composite beam lying on variable elastic foundation. Mechanics Based Design of Structures and Machines 2023: 1-18.
[14] Xie H, Yan G. Some improvements on the energy absorbed in composite plate resting on the viscoelastic substrate. Mechanics Based Design of Structures and Machines 2023;51(11): 6056-75.
[15] Guo Q, Shi G. An accurate and efficient 4-noded quadrilateral plate element for free vibration analysis of laminated composite plates using a refined Third-order Shear Deformation Plate Theory. Composite Structures 2023: 117490.
[16] Chinnaboon B, Panyatong M, Chucheepsakul S. Orthotropic plates resting on viscoelastic foundations with a fractional derivative Kelvin-Voigt model. Composite Structures 2023;322: 117400.
[17] Pham Q-H, Tran VK, Tran TT, Zenkour AM. Nonlocal higher-order finite element modeling for vibration analysis of viscoelastic orthotropic nanoplates resting on variable viscoelastic foundation. Composite Structures 2023;318: 117067.
[18] Monaco GT, Fantuzzi N, Fabbrocino F, Luciano R. Hygro-thermal vibrations and buckling of laminated nanoplates via nonlocal strain gradient theory. Composite Structures 2021;262: 113337.
[19] Alsubaie AM, Alfaqih I, Al-Osta MA, Tounsi A, Chikh A, Mudhaffar IM, Tahir S. Porosity-dependent vibration investigation of functionally graded carbon nanotube-reinforced composite beam. Computers and Concrete 2023;32(1): 75-85.

[20] Madenci E, Ozkilic YO, Hakamy A, Tounsi A. Experimental tensile test and micro-mechanic investigation on carbon nanotube reinforced carbon fiber composite beams. Advances in Nano Research 2023;14(5): 443-50.
[21] Chen S, Xu C, Tong G, Wei X. Free vibration of moderately thick functionally graded plates by a meshless local natural neighbor interpolation method. Engineering Analysis with Boundary Elements 2015;61: 114-26.
[22] Ragb O, Matbuly M, Civalek Ö. Free vibration of irregular plates via indirect differential quadrature and singular convolution techniques. Engineering Analysis with Boundary Elements 2021;128: 66-79.
[23] Van Vinh P. Deflections, stresses and free vibration analysis of bi-functionally graded sandwich plates resting on Pasternak's elastic foundations via a hybrid quasi-3D theory. Mechanics Based Design of Structures and Machines 2023;51(4): 2323-54.
[24] Thai CH, Fereira A, Nguyen-Xuan H, Hung P, Phung-Van P. A nonlocal strain gradient isogeometric model for free vibration analysis of magneto-electro-elastic functionally graded nanoplates. Composite Structures 2023;316: 117005.
[25] Zhang Y-W, Ding H-X, She G-L, Tounsi A. Wave propagation of CNTRC beams resting on elastic foundation based on various higher-order beam theories. Geomechanics and Engineering 2023;33(4): 381-91.
[26] Kumar MB, Sathiya P. Methods and materials for additive manufacturing: A critical review on advancements and challenges. Thin-Walled Structures 2021;159: 107228.
[27] Ong OZS, Ghayesh MH, Losic D. Vibrations of porous functionally graded CNT reinforced viscoelastic beams connected via a viscoelastic layer. International Journal of Engineering Science 2023;191: 103917.
[28] Njim EK, Al-Waily M, Bakhy SH. A critical review of recent research of free vibration and stability of functionally graded materials of sandwich plate. IOP Conference Series: Materials Science and Engineering: IOP Publishing; 2021. 012081.
[29] Hellal H, Bourada M, Hebali H, Bourada F, Tounsi A, Bousahla AA, Mahmoud SR. Dynamic and stability analysis of functionally graded material sandwich plates in hygro-thermal environment using a simple higher shear deformation theory. Journal of Sandwich Structures & Materials 2021;23(3): 814-51.
[30] Dung NT, Minh PV, Hung HM, Tien DM. The third-order shear deformation theory for modeling the static bending and dynamic responses of piezoelectric bidirectional functionally graded plates. Advances in Materials Science and Engineering 2021;2021: 1-15.
[31] Ali MI, Azam M, Ranjan V, Banerjee J. Free vibration of sigmoid functionally graded plates using the dynamic stiffness method and the Wittrick-Williams algorithm. Computers & Structures 2021;244: 106424.
[32] Chen X, Chen L, Huang S, Li M, Li X. Nonlinear forced vibration of in-plane bi-directional functionally graded materials rectangular plate with global and localized geometrical imperfections. Applied Mathematical Modelling 2021;93: 443-66.
[33] Katiyar V, Gupta A. Vibration response of a geometrically discontinuous bi-directional functionally graded plate resting on elastic foundations in thermal environment with initial imperfections. Mechanics Based Design of Structures and Machines 2023;51(6): 3480-508.
[34] Seyfi A, Aghdam M. Vibrational behavior of temperature-dependent imperfect functionally graded plate lying on an elastic substrate. Mechanics Based Design of Structures and Machines 2023;51(7): 3868-89.
[35] Raza A, Pathak H, Talha M. Influence of microstructural defects on free flexural vibration of cracked functionally graded plates in thermal medium using XFEM. Mechanics Based Design of Structures and Machines 2023;51(12): 6774-97.

[36] Avey M, Kadioglu F. On the primary resonance of laminated moderately-thick plates containing of heterogeneous nanocomposite layers considering nonlinearity. Composite Structures 2023;322: 117377.
[37] Hoang VNV, Thanh PT. Influences of arbitrary-distributed Kerr foundation on free vibration and nonlinear transient response of functionally graded plate in thermal environment. Thin-Walled Structures 2023;188: 110802.
[38] Rajasekaran S, Khaniki HB, Ghayesh MH. Thermo-mechanics of multi-directional functionally graded elastic sandwich plates. Thin-Walled Structures 2022;176: 109266.
[39] Iijima S. Helical microtubules of graphitic carbon. Nature 1991;354(6348): 56-58.
[40] Mohd Nurazzi N, Asyraf MM, Khalina A, Abdullah N, Sabaruddin FA, Kamarudin SH, Ahmad Sb, Mahat AM, Lee CL, Aisyah H. Fabrication, functionalization, and application of carbon nanotube-reinforced polymer composite: An overview. Polymers 2021;13(7): 1047.
[41] Ong OZS, Ghayesh MH, Losic D, Amabili M. Coupled dynamics of double beams reinforced with bidirectional functionally graded carbon nanotubes. Engineering Analysis with Boundary Elements 2022;143: 263-82.
[42] Mangalasseri AS, Mahesh V, Mukunda S, Ponnusami S, Harursampath D, Tounsi A. Vibration based energy harvesting performance of magnetoelectro-elastic beams reinforced with carbon nanotubes. Advances in Nano Research 2023;14(1): 27-43.
[43] Maheswaran R, Shanmugavel BP. A critical review of the role of carbon nanotubes in the progress of next-generation electronic applications. Journal of Electronic Materials 2022;51(6): 2786-800.
[44] Lei Z, Zhang L, Liew K. Vibration of FG-CNT reinforced composite thick quadrilateral plates resting on pasternak foundations. Engineering Analysis with Boundary Elements 2016;64: 1-11.
[45] Ong OZS, Ghayesh MH, Losic D. Dynamical behaviour of CNT reinforced plates with mass imperfections. Procedia Structural Integrity 2023;45: 140-47.
[46] Ly D-K, Truong TT, Nguyen S-N, Nguyen-Thoi T. A smoothed finite element formulation using zig-zag theory for hybrid damping vibration control of laminated functionally graded carbon nanotube reinforced composite plates. Engineering Analysis with Boundary Elements 2022;144: 456-74.
[47] Dogan A. Dynamic response of laminated functionally graded carbon nanotube-reinforced composite viscoelastic plates. Mechanics Based Design of Structures and Machines 2023: 1-28.
[48] Arshid E, Khorasani M, Soleimani-Javid Z, Amir S, Tounsi A. Porosity-dependent vibration analysis of FG microplates embedded by polymeric nanocomposite patches considering hygrothermal effect via an innovative plate theory. Engineering with Computers 2021: 1-22.
[49] Huang Y, Karami B, Shahsavari D, Tounsi A. Static stability analysis of carbon nanotube reinforced polymeric composite doubly curved micro-shell panels. Archives of Civil and Mechanical Engineering 2021;21(4): 1-15.
[50] Civalek Ö, Dastjerdi S, Akgöz B. Buckling and free vibrations of CNT-reinforced cross-ply laminated composite plates. Mechanics Based Design of Structures and Machines 2022;50(6): 1914-31.
[51] Kumar R, Jana P. Exact modal analysis of multilayered FG-CNT plate assemblies using the dynamic stiffness method. Mechanics of Advanced Materials and Structures 2022: 1-20.
[52] Dat ND, Thanh NV, MinhAnh V, Duc ND. Vibration and nonlinear dynamic analysis of sandwich FG-CNTRC plate with porous core layer. Mechanics of Advanced Materials and Structures 2022;29(10): 1431-48.
[53] Khaniki HB, Ghayesh MH. A review on the mechanics of carbon nanotube strengthened deformable structures. Engineering Structures 2020;220: 110711.

[54] Zhang Y, Shi D, He D, Shao D. Free vibration analysis of laminated composite double-plate structure system with elastic constraints based on improved fourier series method. Shock and Vibration 2021;2021: 1-25.
[55] Oniszczuk Z. Free transverse vibrations of an elastically connected rectangular simply supported double-plate complex system. Journal of Sound and Vibration 2000;236(4): 595-608.
[56] Oniszczuk Z. Forced transverse vibrations of an elastically connected complex rectangular simply supported double-plate system. Journal of Sound and Vibration 2004;270(4-5): 997-1011.
[57] Wen S, Chen M, Zhou Z, Jia W. Analytical and experimental studies for the vibration transmission of the double-plated structure containing the inner fluid and elastic connections. Thin-Walled Structures 2023;188: 110806.
[58] Cao TNT, Reddy J, Lieu QX, Nguyen XV, Luong VH. A multi-layer moving plate method for dynamic analysis of viscoelastically connected double-plate systems subjected to moving loads. Advances in Structural Engineering 2021;24(9): 1798-813.
[59] Heidari E, Ariaei A. A new approach for free vibration analysis of a system of elastically interconnected similar rectangular plates. Earthquake Engineering and Engineering Vibration 2022;21(4): 947-67.
[60] Shen H-S. Nonlinear bending of functionally graded carbon nanotube-reinforced composite plates in thermal environments. Composite Structures 2009;91(1): 9-19.
[61] Zhu P, Lei Z, Liew KM. Static and free vibration analyses of carbon nanotube-reinforced composite plates using finite element method with first order shear deformation plate theory. Composite Structures 2012;94(4): 1450-60.
[62] Shen H-S. Postbuckling of nanotube-reinforced composite cylindrical shells in thermal environments, Part I: Axially-loaded shells. Composite Structures 2011;93(8): 2096-108.
[63] Natarajan S, Haboussi M, Manickam G. Application of higher-order structural theory to bending and free vibration analysis of sandwich plates with CNT reinforced composite facesheets. Composite Structures 2014;113: 197-207.
[64] Han Y, Elliott J. Molecular dynamics simulations of the elastic properties of polymer/carbon nanotube composites. Computational Materials Science 2007;39(2): 315-23.
[65] Bauchau O, Craig J. Kirchhoff plate theory. Structural Analysis 2009: 819-914.
[66] Selim B, Zhang L, Liew K. Vibration analysis of CNT reinforced functionally graded composite plates in a thermal environment based on Reddy's higher-order shear deformation theory. Composite Structures 2016;156: 276-90.
[67] Mellouli H, Mallek H, Wali M, Dammak F. Finite rotation RPIM formulation for geometrically nonlinear analysis of FG-CNTRC shell structure. Advances in Materials, Mechanics and Manufacturing II: Proceedings of the Third International Conference on Advanced Materials, Mechanics and Manufacturing (A3M'2021), March 25-27, 2021: Springer; 2022. 201-08.

Table 1: Natural frequencies of simplified plate models obtained using the current method of the study and (a) existing literature on carbon nanotubes reinforced *single* plate [66]; (b) existing literature on *non*-reinforced double plates (rad/s) [55]; (c) the FEM on *non*-reinforced double plates (Hz).

(a)

Functionally graded	Mode	Literature	Theory	Mode	Literature	Theory
		$V_{CNT}^{'} = 0.11$			$V_{CNT}^{'} = 0.14$	
UD	1	19.197	19.574	1	21.363	21.889
	2	23.375	23.684	2	25.293	25.747
	3	34.626	34.481	3	36.250	36.231
FG-O	1	14.265	14.416	1	15.785	15.992
	2	19.338	19.426	2	20.546	20.689
	3	31.584	31.238	3	32.495	32.194
FG-X	1	22.954	23.642	1	25.555	26.516
	2	26.741	27.352	2	29.175	30.052
	3	37.528	37.652	3	39.791	40.147
		$V_{CNT}^{'} = 0.17$				
UD	1	23.659	24.108			
	2	28.942	29.304			
	3	43.106	42.902			
FG-O	1	17.502	17.675			
	2	23.745	23.848			
	3	38.823	38.396			
FG-X	1	28.345	29.180			
	2	33.354	34.077			
	3	47.444	47.538			

(b)

Mode	Literature	Theory	Mode	Literature	Theory	Mode	Literature	Theory
$\omega_{1,11}$	52.8	52.8	$\omega_{1,12}$	84.5	84.5	$\omega_{1,13}$	137.3	137.3
$\omega_{2,11}$	72	72.0	$\omega_{2,12}$	97.7	97.6	$\omega_{2,13}$	145.8	145.7
$\omega_{1,21}$	179.5	179.5	$\omega_{1,22}$	211.2	211.1	$\omega_{1,23}$	264	263.9
$\omega_{2,21}$	186.1	186.0	$\omega_{2,22}$	216.8	216.8	$\omega_{2,23}$	268.5	268.4
$\omega_{1,31}$	390.7	390.6	$\omega_{1,32}$	422.4	422.2	$\omega_{1,33}$	475.2	475.0
$\omega_{2,31}$	393.8	393.6	$\omega_{2,32}$	425.2	425.0	$\omega_{2,33}$	477.7	477.5

(c)

Mode	FEM	Theory	Mode	FEM	Theory
$\omega_{1,11}$	48.1	48.0	$\omega_{1,12}$	120.3	119.9
$\omega_{2,11}$	54.2	54.3	$\omega_{2,12}$	122.8	122.6
$\omega_{1,21}$	120.3	119.9	$\omega_{1,22}$	192.2	191.9
$\omega_{2,21}$	122.8	122.6	$\omega_{2,22}$	193.8	193.6

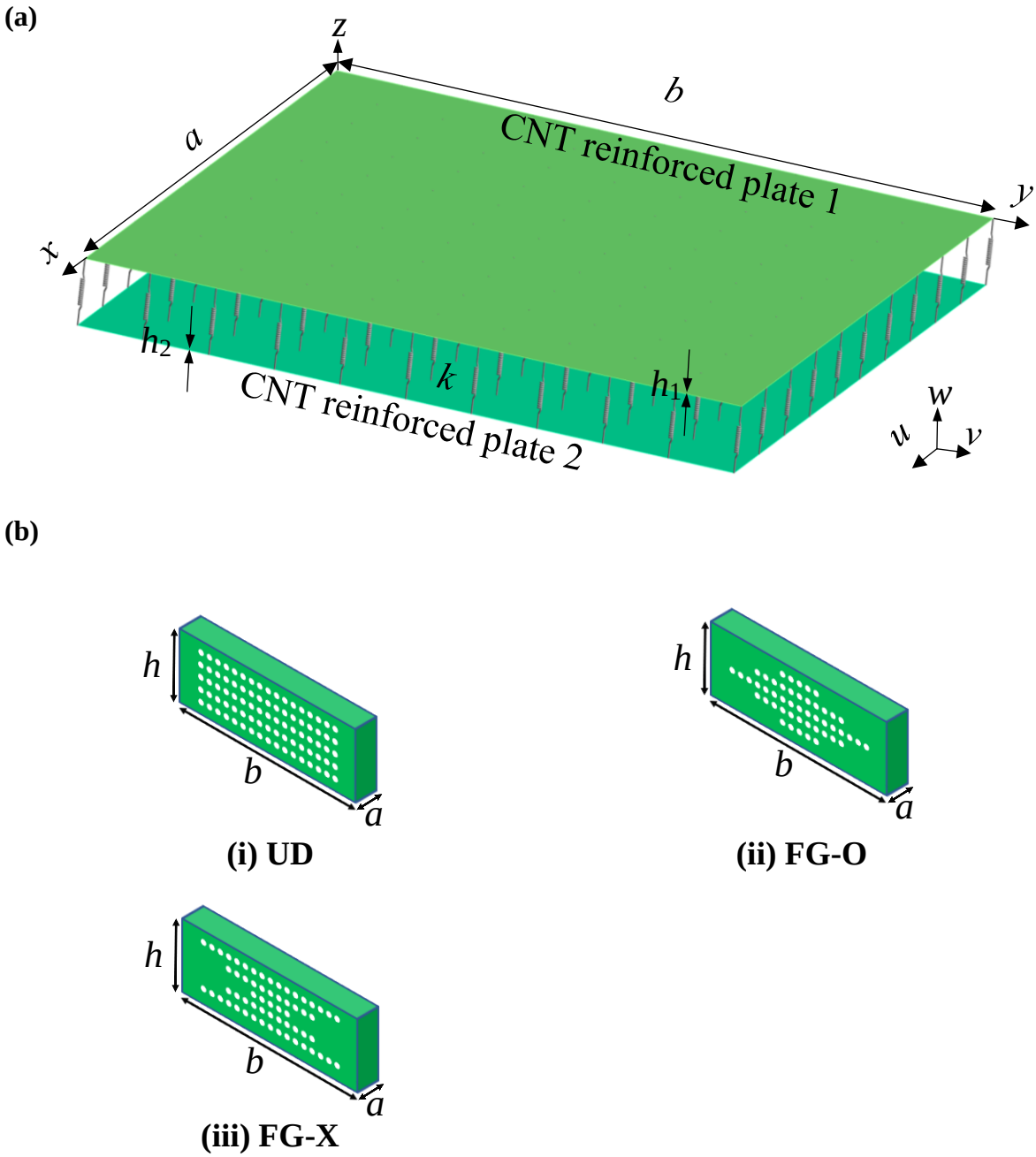

Fig. 1: (a) Simply supported functionally graded carbon nanotubes reinforced rectangular double plates; (b) carbon nanotubes reinforced patterns.

(a)

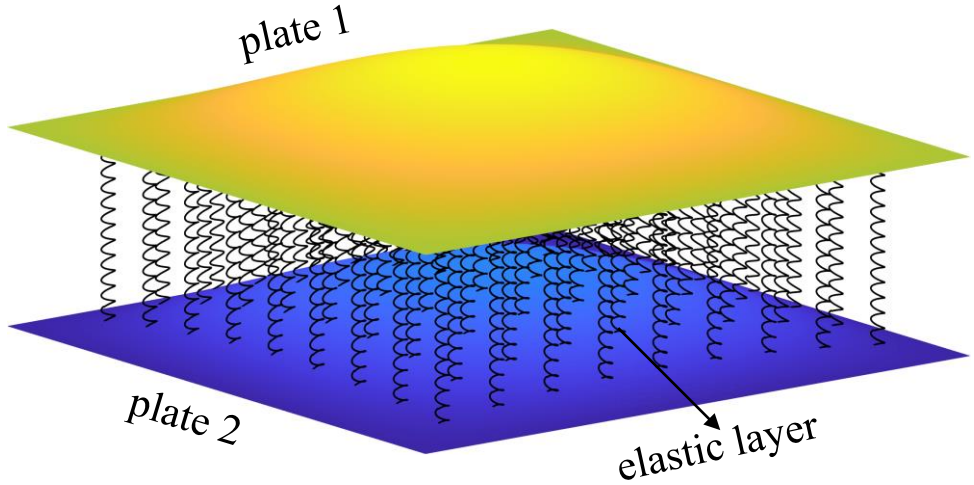

(b)

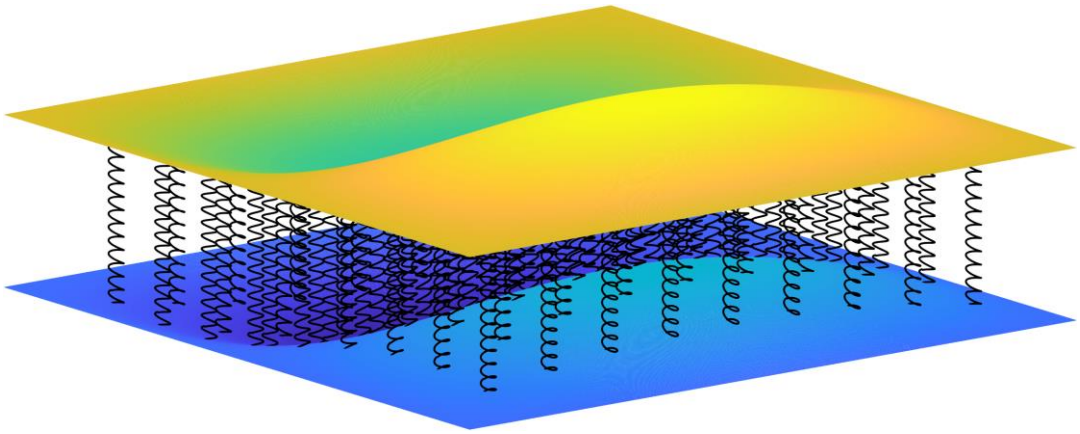

(c)

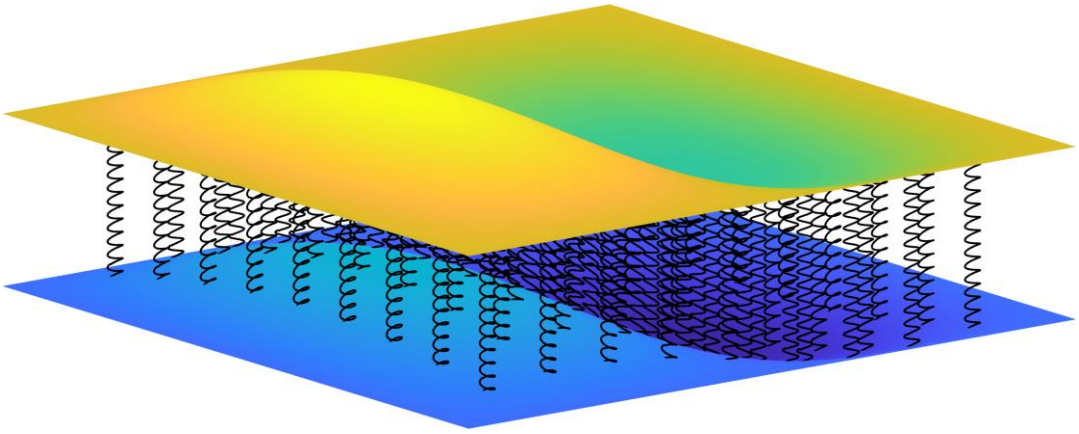

(d)

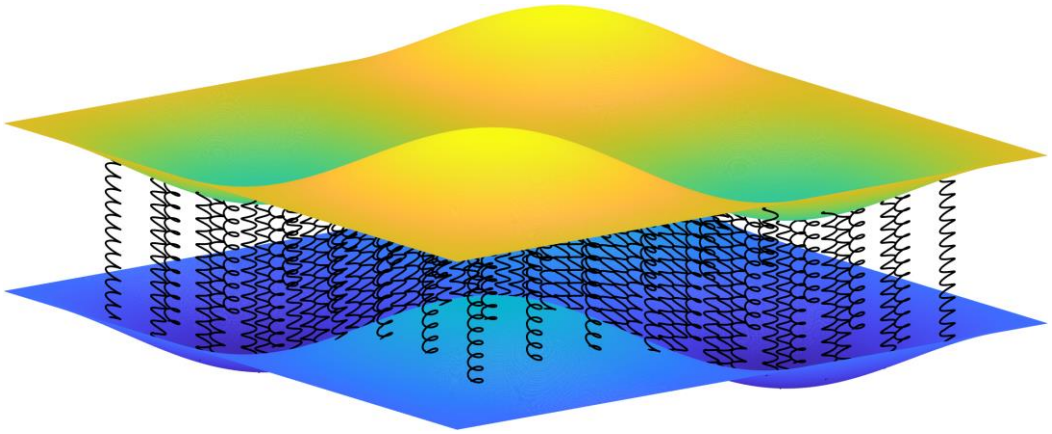

Fig. 2: MDM based *first* series mode shapes of *non*-carbon-nanotube reinforced square double plates, (a) $\omega_{1,11}$; (b) $\omega_{1,12}$; (c) $\omega_{1,21}$; (d) $\omega_{1,22}$.

(a)

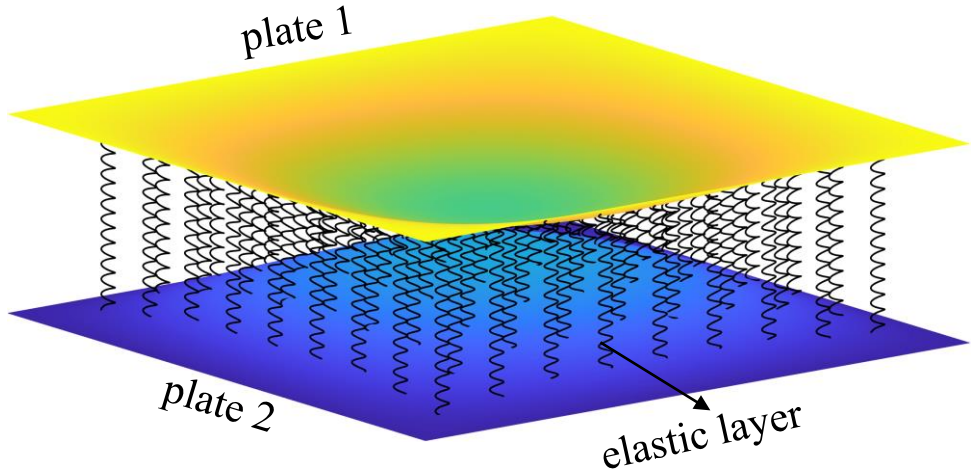

(b)

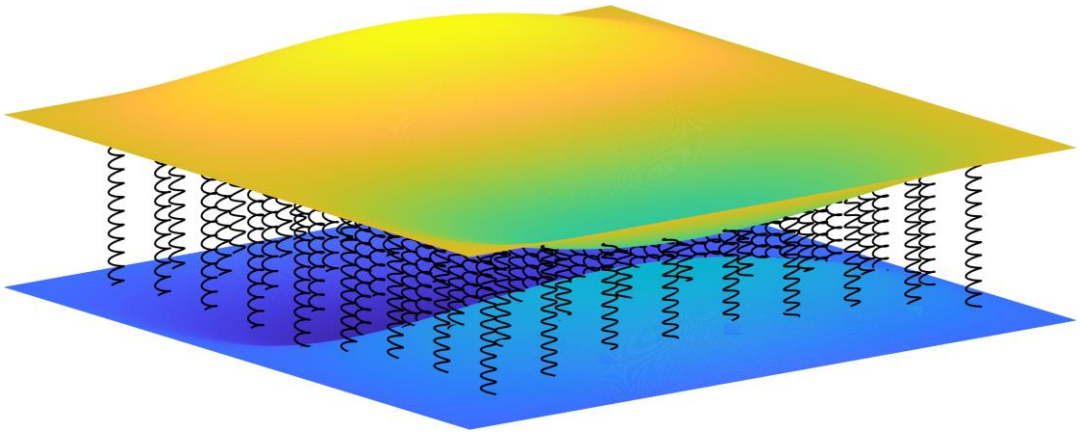

(c)

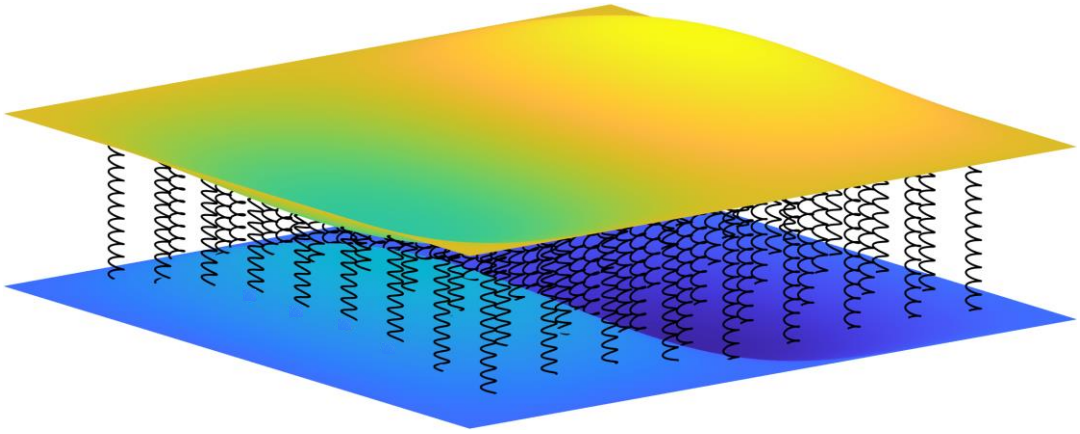

(d)

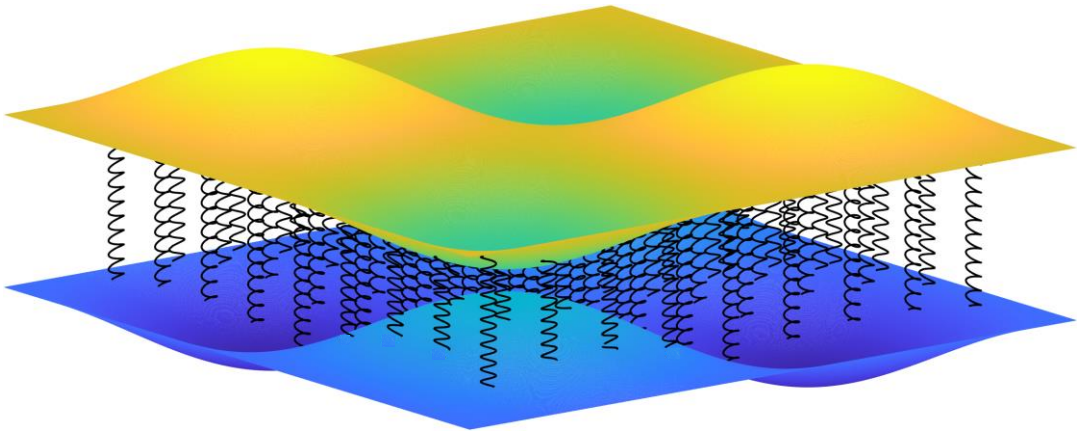

Fig. 3: MDM based *second* series mode shapes of *non*-carbon-nanotube reinforced square double plates, (a) $\omega_{2,11}$; (b) $\omega_{2,12}$; (c) $\omega_{2,21}$; (d) $\omega_{2,22}$.

(a)

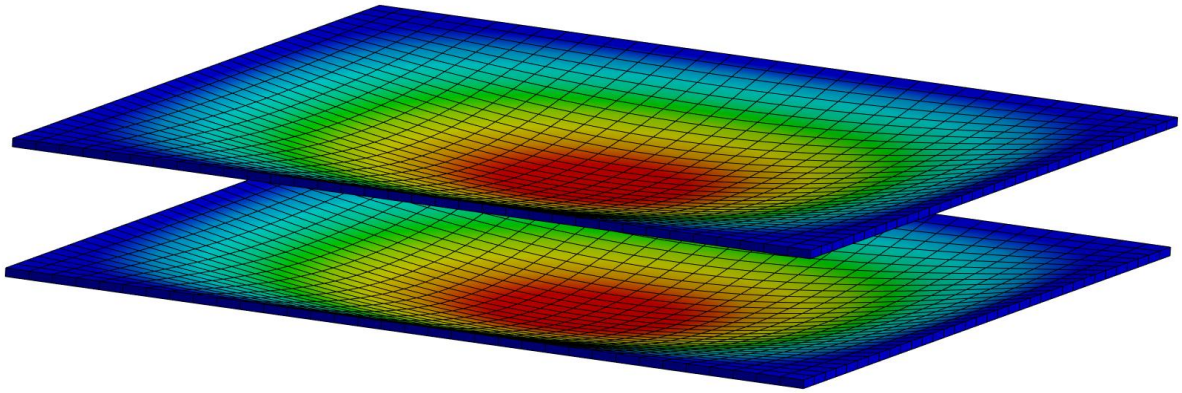

(b)

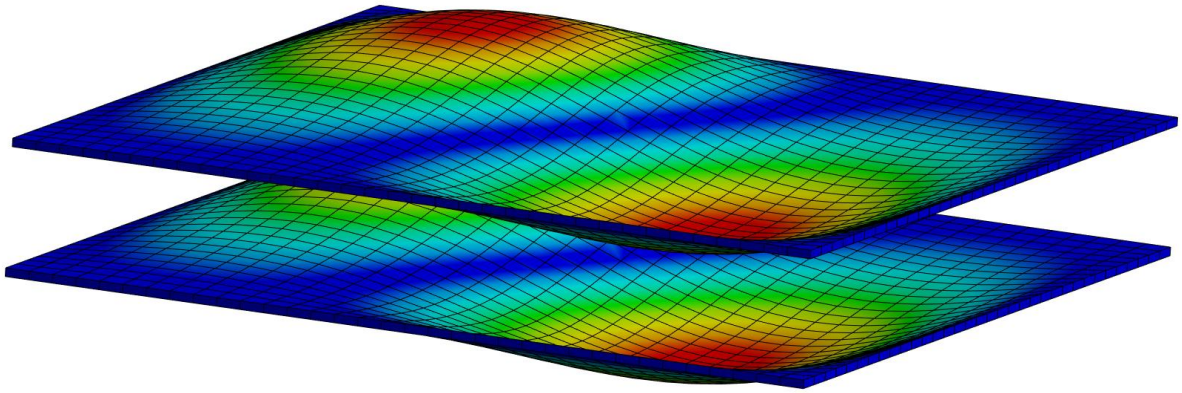

(c)

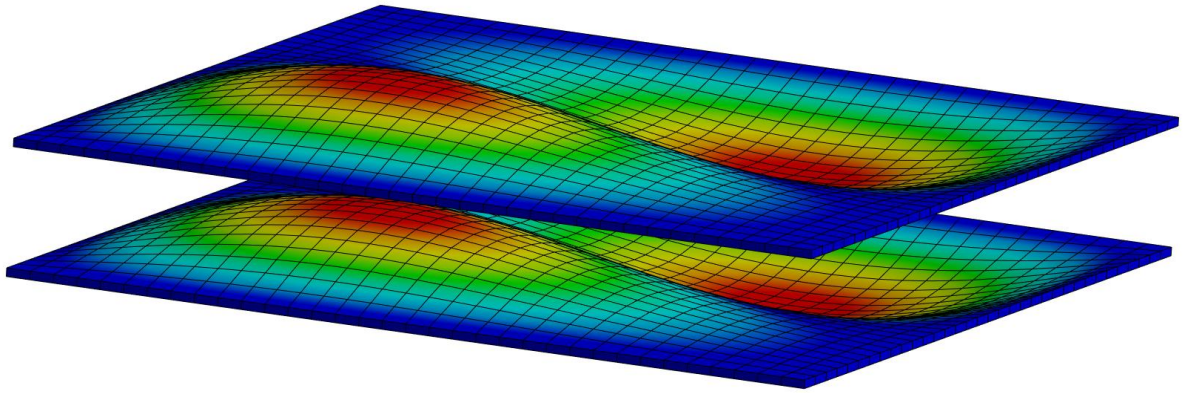

(d)

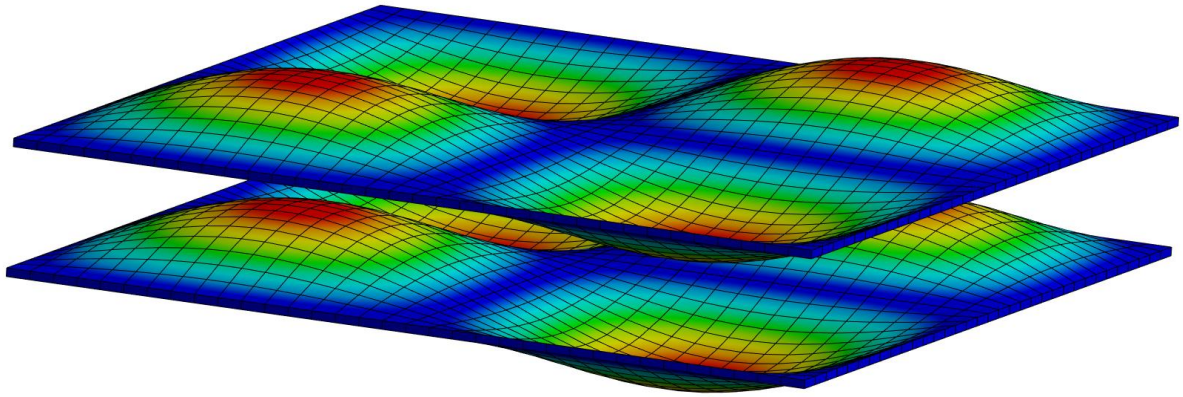

Fig. 4: FEM based *first* series mode shapes of *non*-carbon-nanotube reinforced square double plates, (a) $\omega_{1,11}$; (b) $\omega_{1,12}$; (c) $\omega_{1,21}$; (d) $\omega_{1,22}$.

(a)

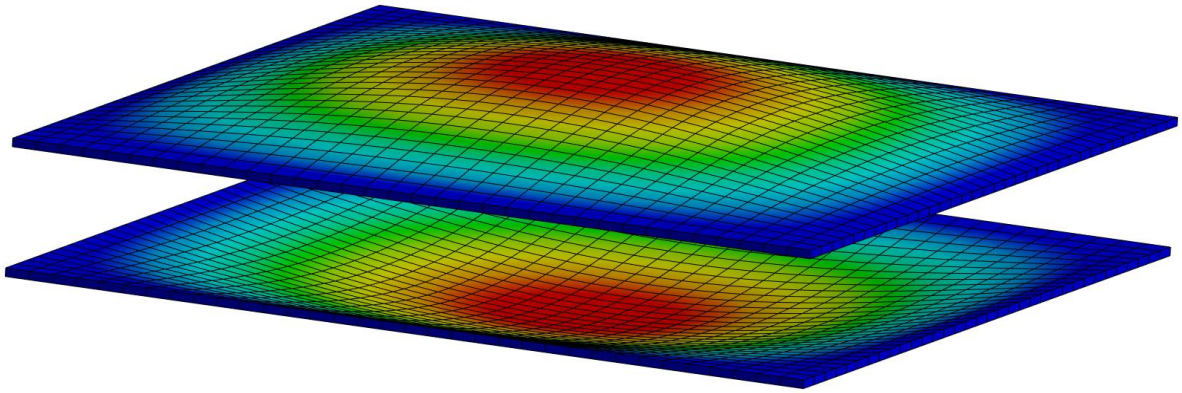

(b)

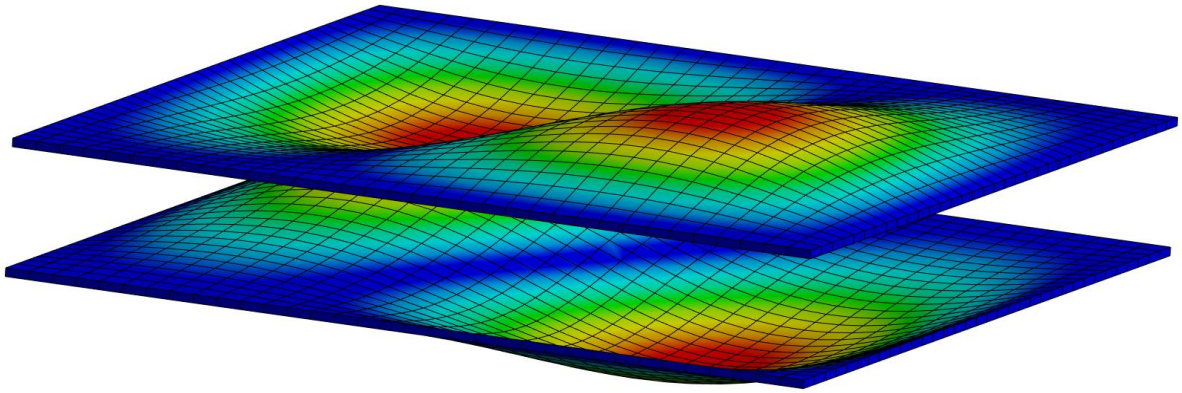

(c)

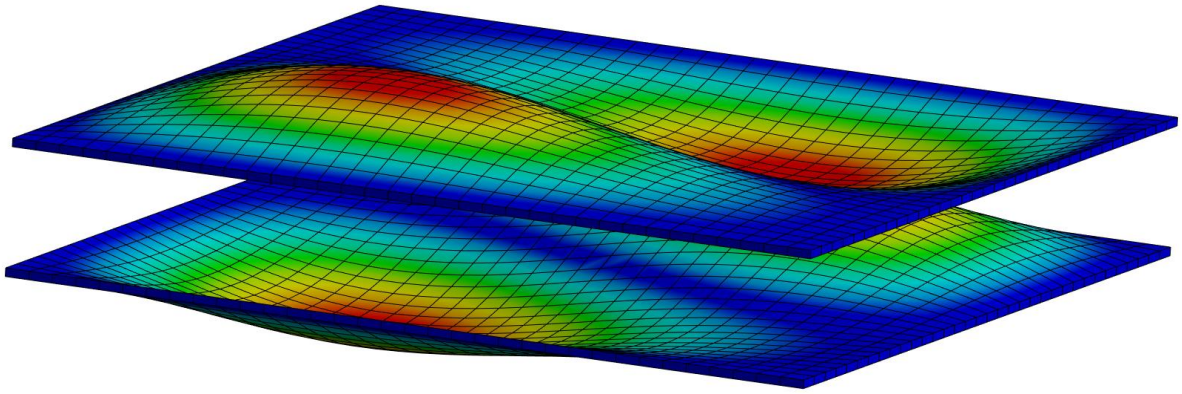

(d)

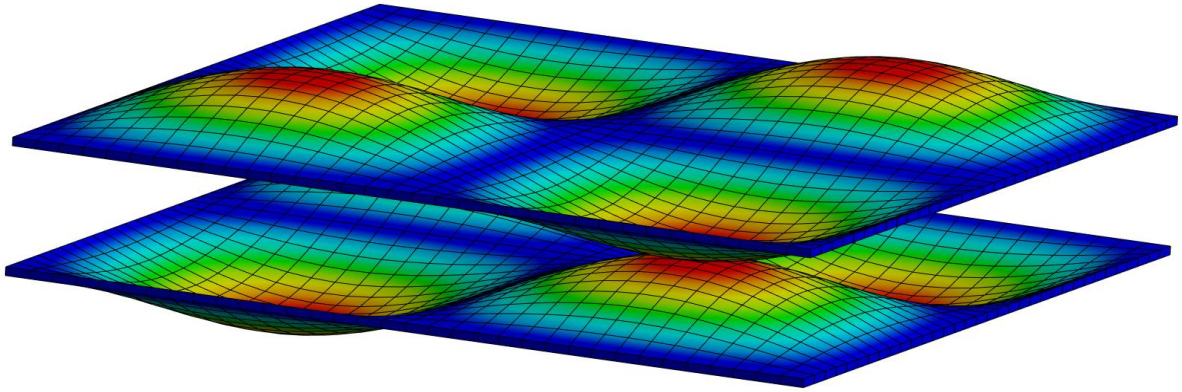

Fig. 5: FEM based *second* series mode shapes of *non*-carbon-nanotube reinforced square double plates, (a) $\omega_{2,11}$; (b) $\omega_{2,12}$; (c) $\omega_{2,21}$; (d) $\omega_{2,22}$.

(a)

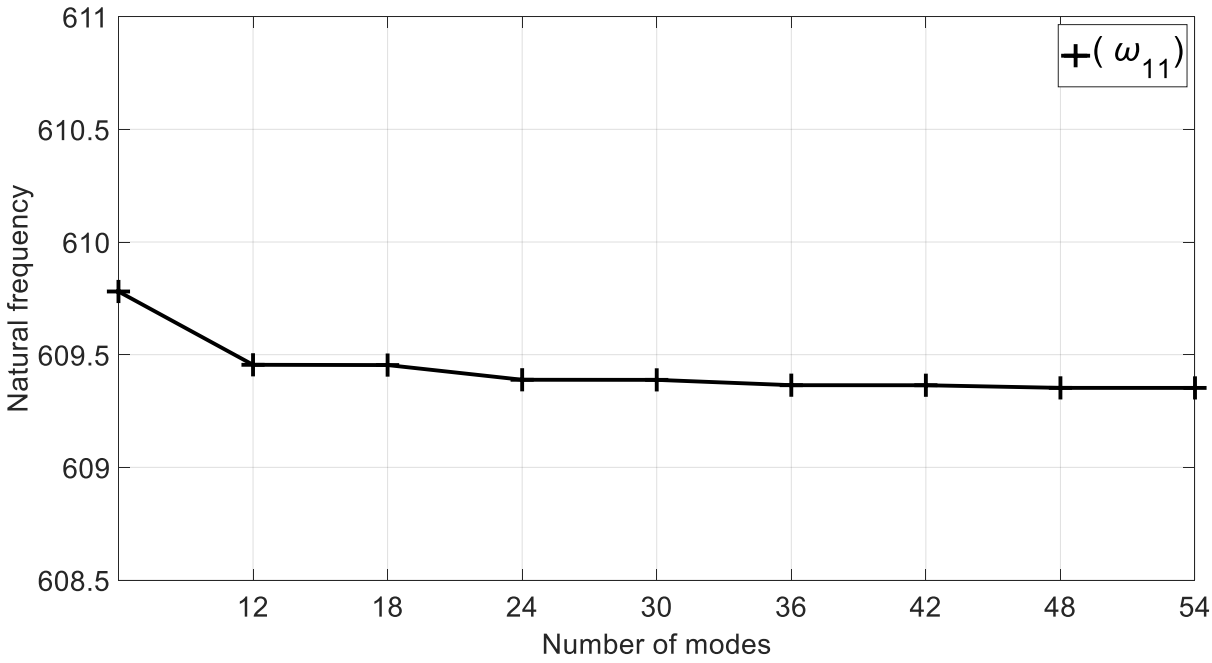

(b)

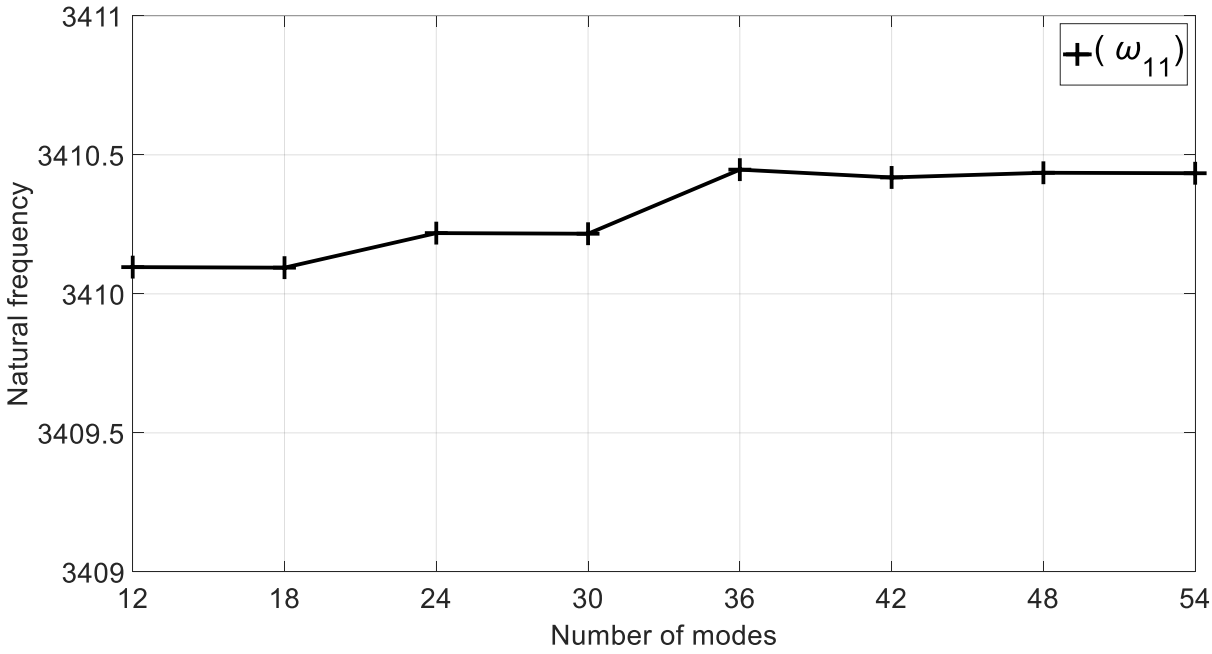

Fig. 6: Convergence of the fundamental natural frequencies for functionally graded carbon nanotubes reinforced square double plates, (a) lateral-motion natural frequency; (b) axial-motion natural frequency.

(a)

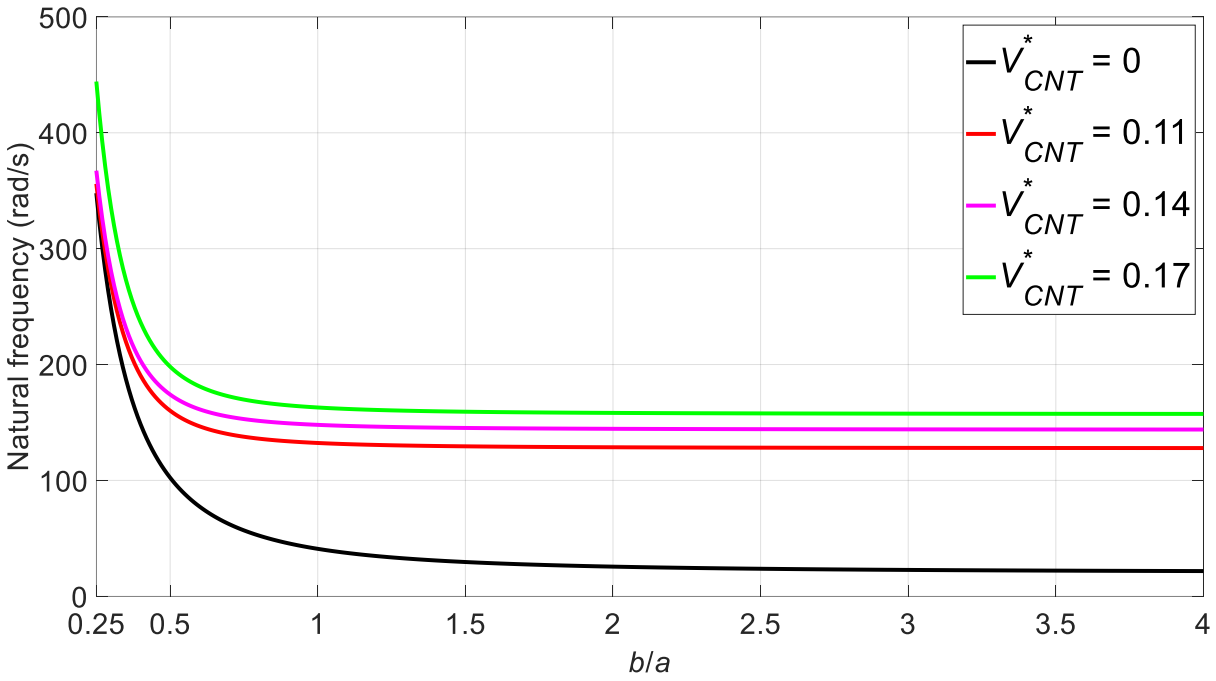
Natural frequency (rad/s)
b/a
V^*_{CNT} = 0
V^*_{CNT} = 0.11
V^*_{CNT} = 0.14
V^*_{CNT} = 0.17

(b)

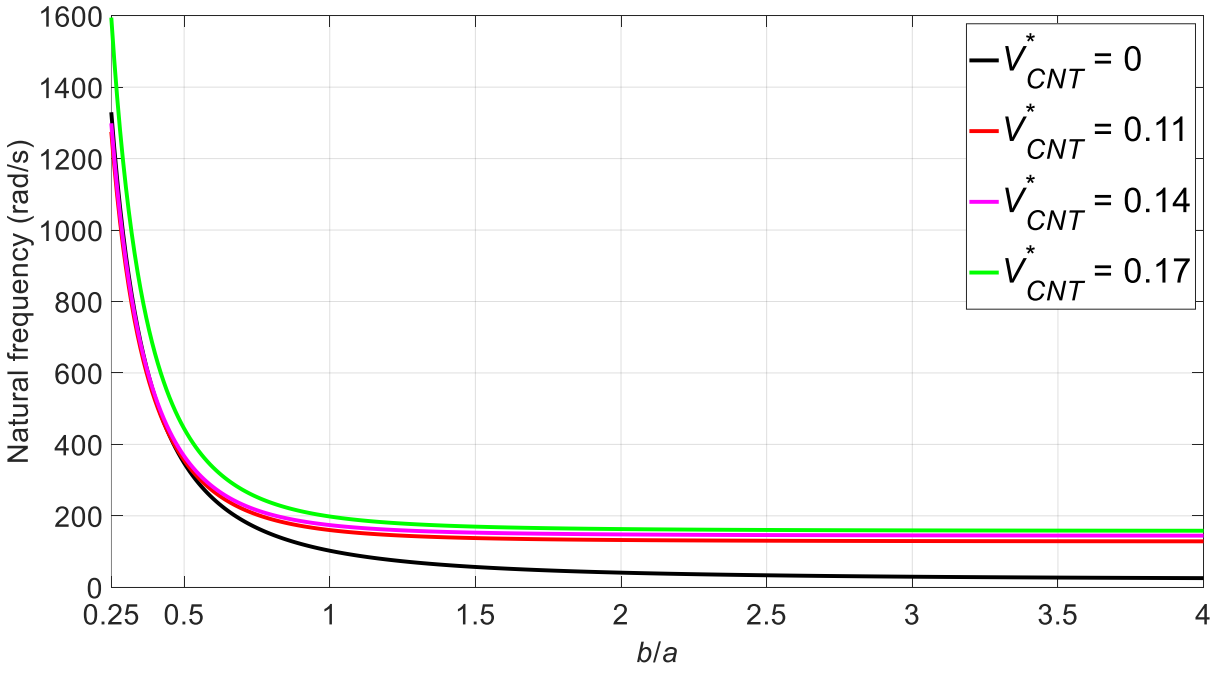
Natural frequency (rad/s)
b/a
V^*_{CNT} = 0
V^*_{CNT} = 0.11
V^*_{CNT} = 0.14
V^*_{CNT} = 0.17

(c)

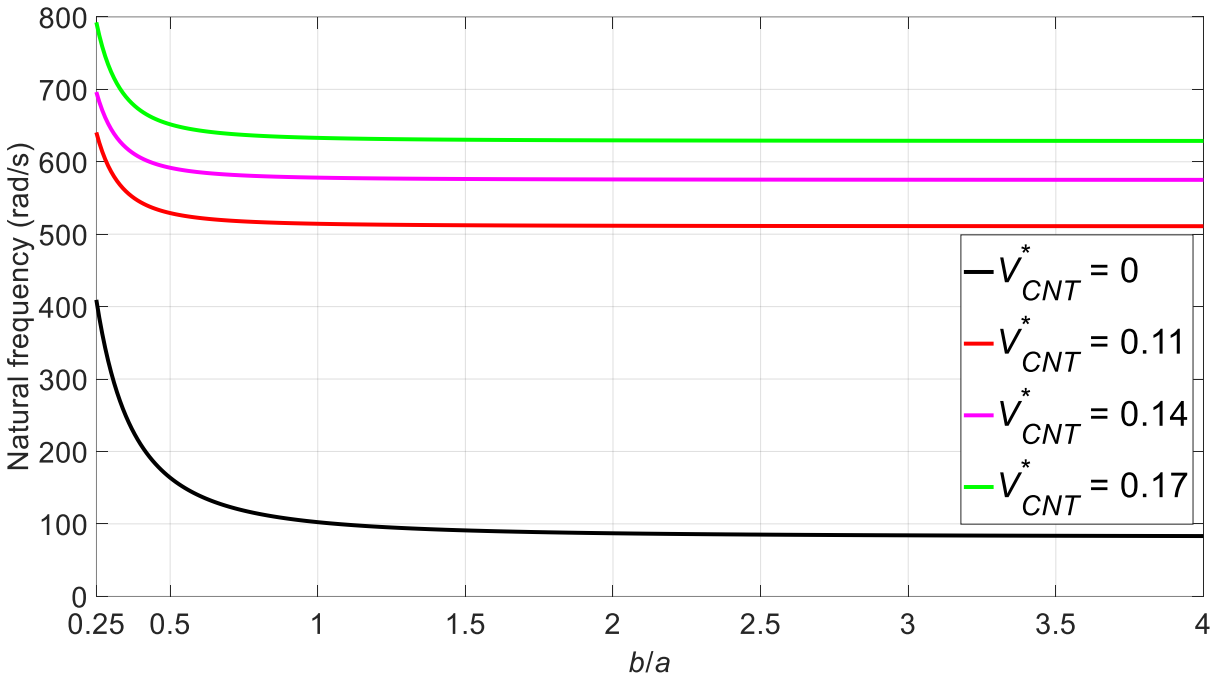

(d)

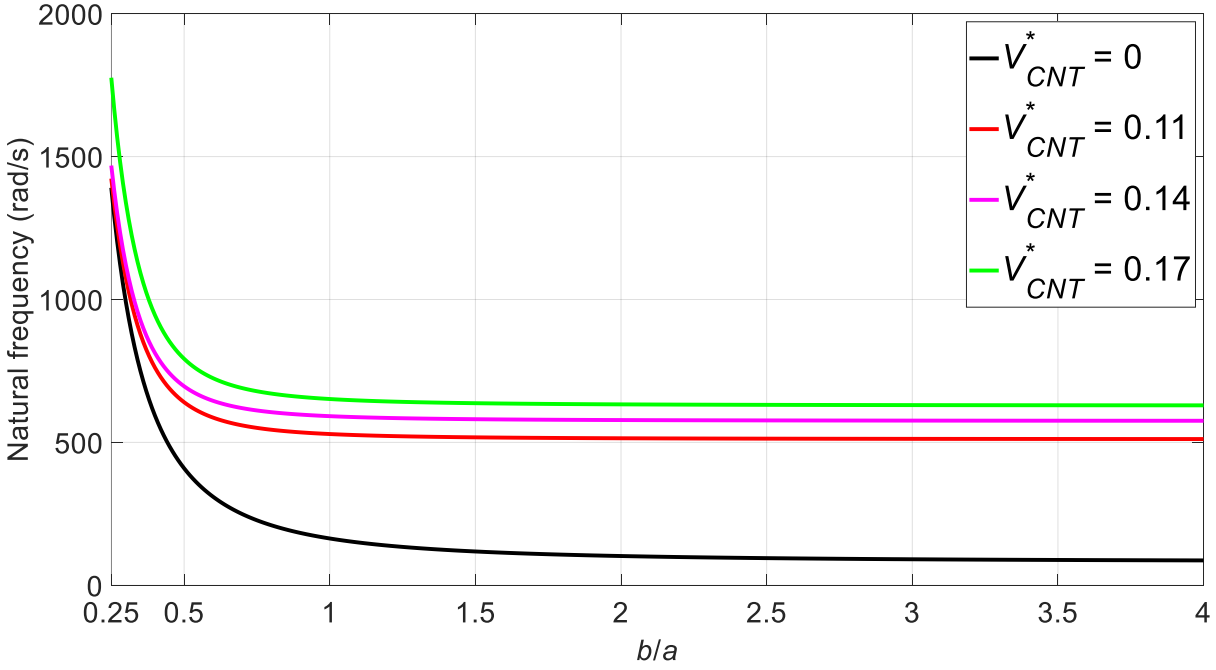

Fig. 7: Aspect ratio effects on the *first* series dimensional transverse-motion natural frequencies of a UD carbon nanotubes reinforced rectangular double plates, (a) $\omega_{1,11}$; (b) $\omega_{1,12}$; (c) $\omega_{1,21}$; (d) $\omega_{1,22}$.

(a)

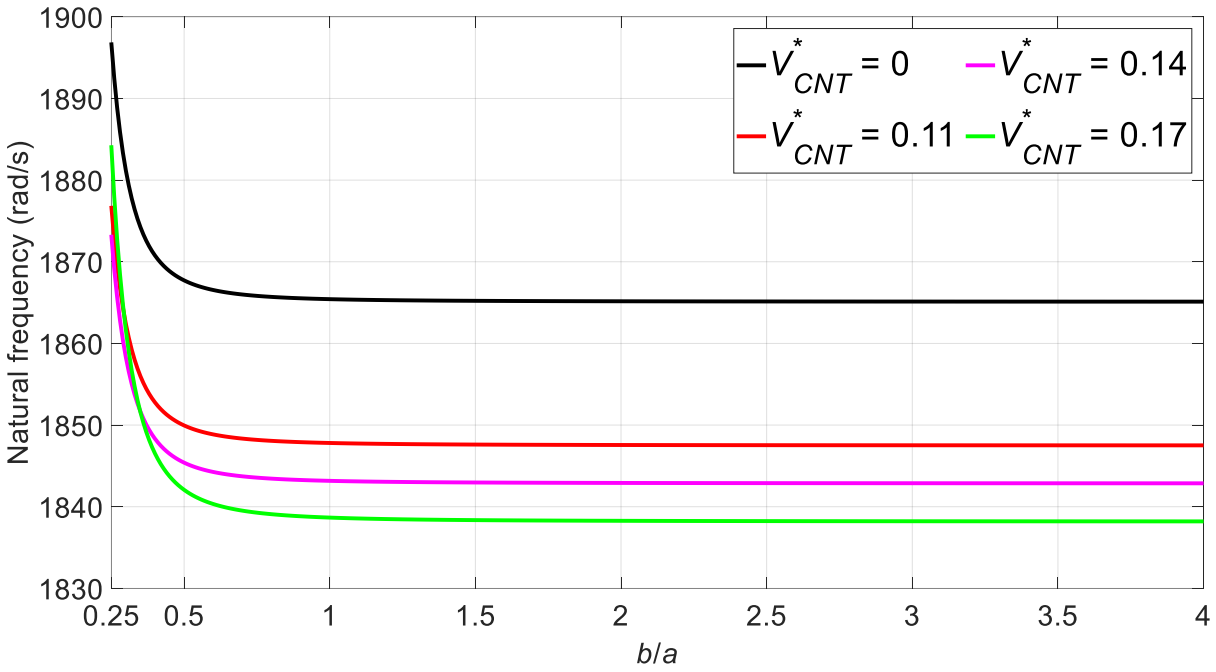
1900
1890
1880
1870
1860
1850
1840
1830
Natural frequency (rad/s)
0.25
0.5
1
1.5
2
2.5
3
3.5
4
b/a
V^*_{CNT} = 0
V^*_{CNT} = 0.14
V^*_{CNT} = 0.11
V^*_{CNT} = 0.17

(b)

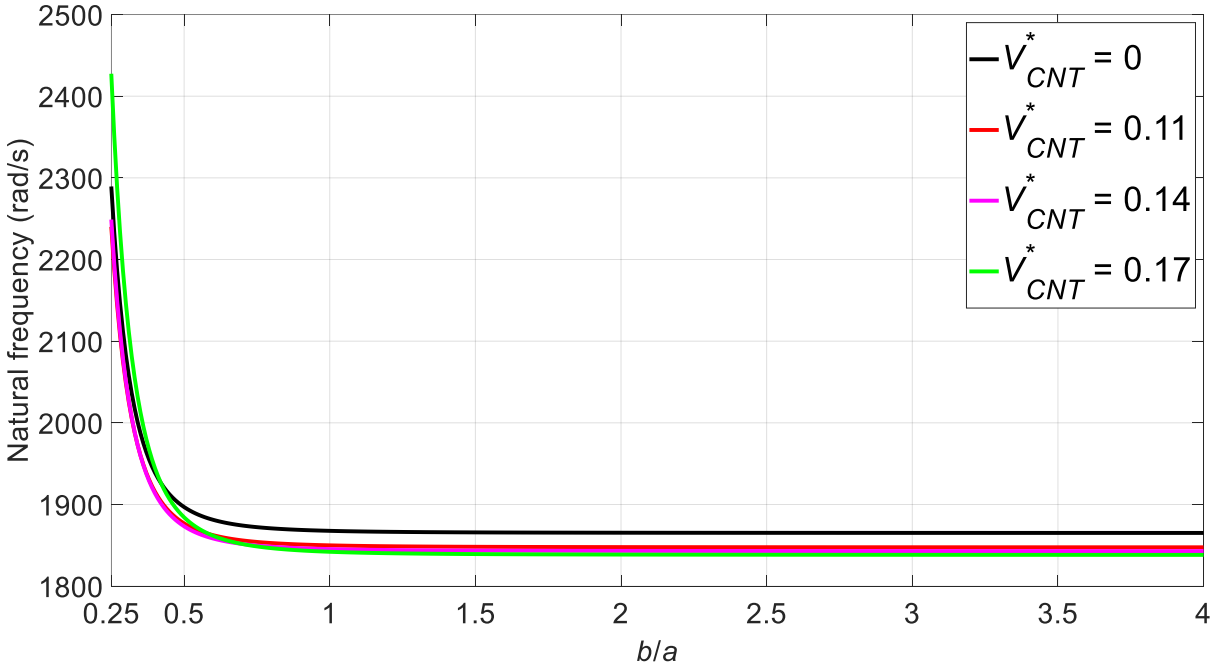
2500
2400
2300
2200
2100
2000
1900
1800
Natural frequency (rad/s)
0.25
0.5
1
1.5
2
2.5
3
3.5
4
b/a
V^*_{CNT} = 0
V^*_{CNT} = 0.11
V^*_{CNT} = 0.14
V^*_{CNT} = 0.17

(c)

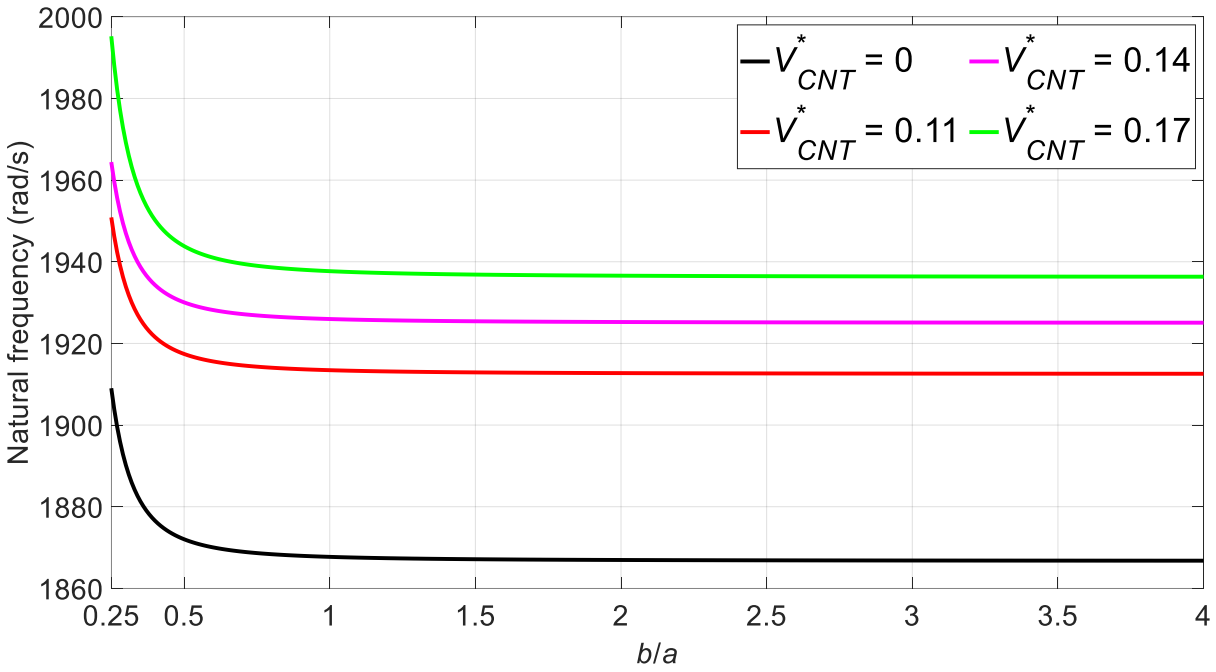

(d)

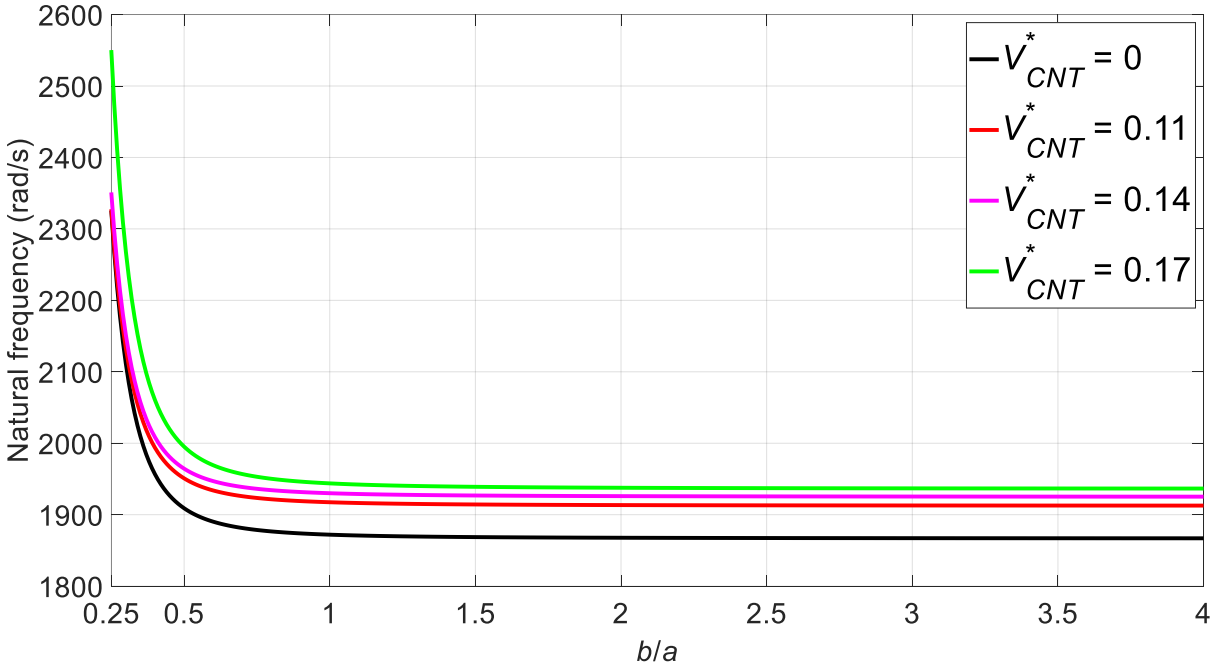

Fig. 8: Aspect ratio effects on the *second* series dimensional transverse-motion natural frequencies of a UD carbon nanotubes reinforced rectangular double plates, (a) $\omega_{2,11}$; (b) $\omega_{2,12}$; (c) $\omega_{2,21}$; (d) $\omega_{2,22}$.

(a)

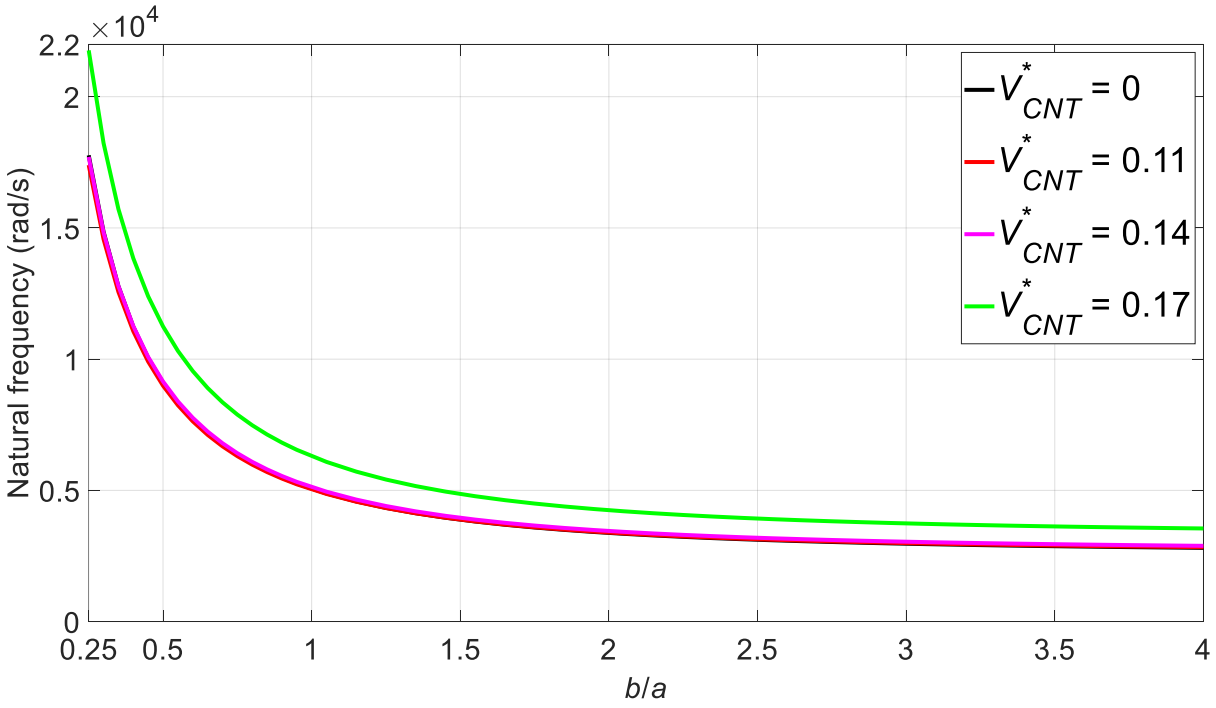

(b)

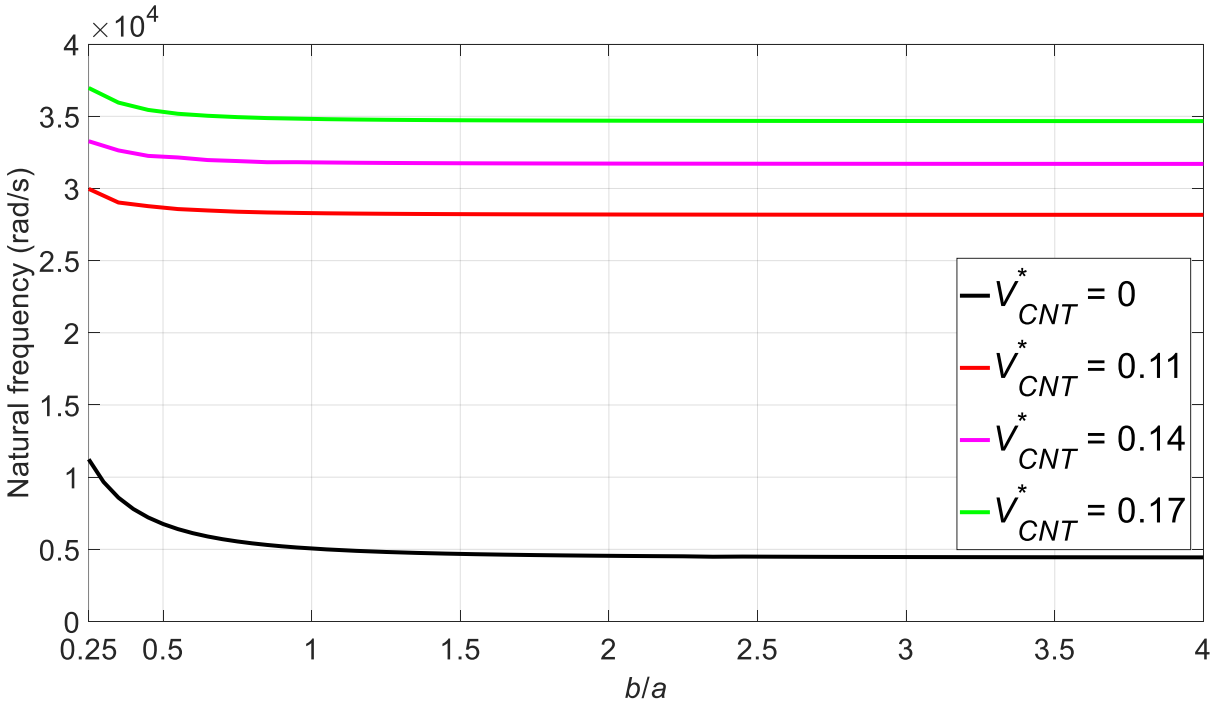

Fig. 9: Aspect ratio effects on the dimensional natural frequencies of a UD carbon nanotubes reinforced rectangular double plates, (a) lateral-motion natural frequency; (b) axial-motion natural frequency.

(a)

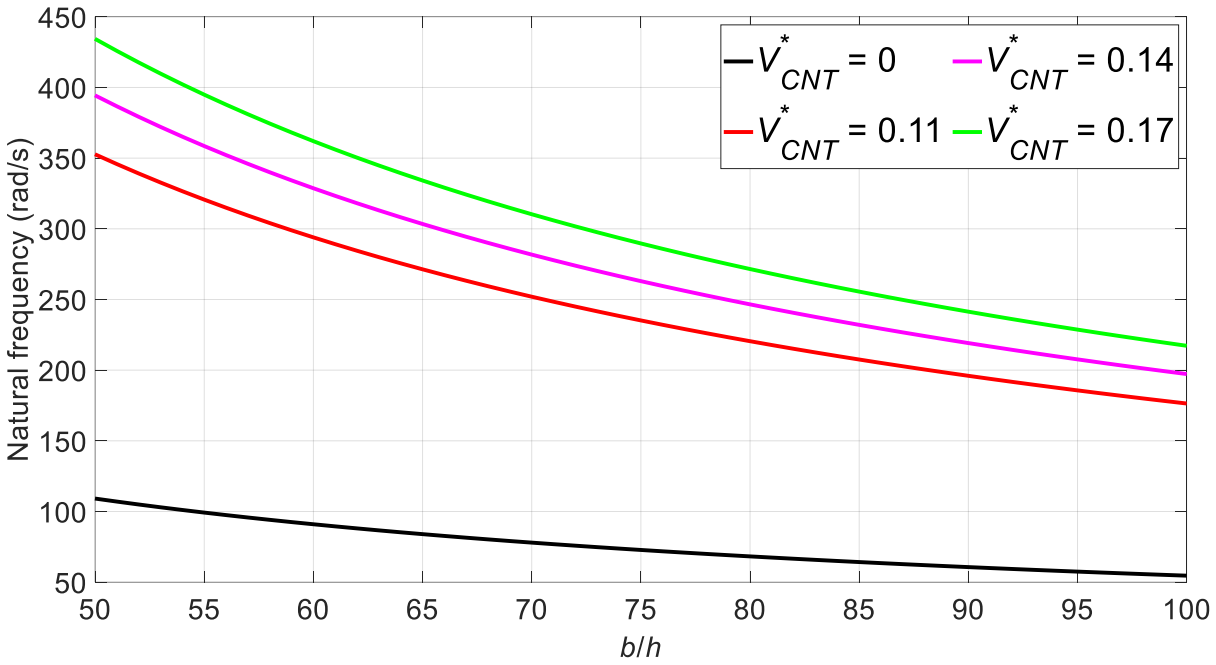
Natural frequency (rad/s)
450
400
350
300
250
200
150
100
50
50
55
60
65
70
75
80
85
90
95
100
b/h
V^*_{CNT} = 0
V^*_{CNT} = 0.14
V^*_{CNT} = 0.11
V^*_{CNT} = 0.17

(b)

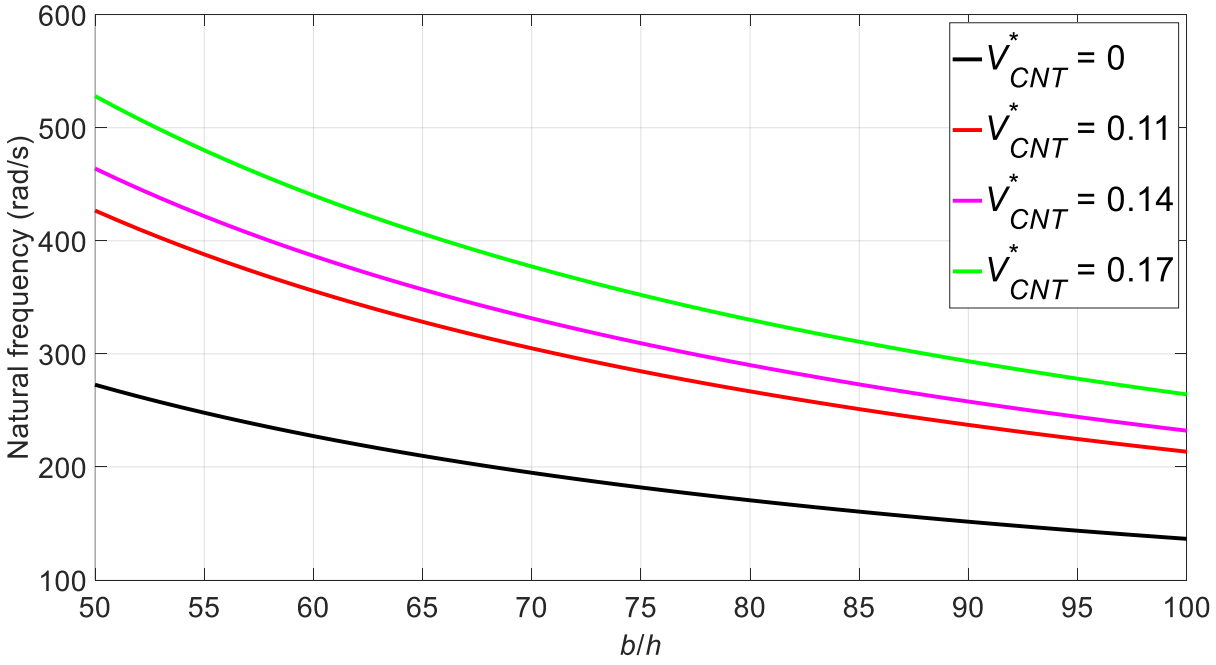
Natural frequency (rad/s)
600
500
400
300
200
100
50
55
60
65
70
75
80
85
90
95
100
b/h
V^*_{CNT} = 0
V^*_{CNT} = 0.11
V^*_{CNT} = 0.14
V^*_{CNT} = 0.17

(c)

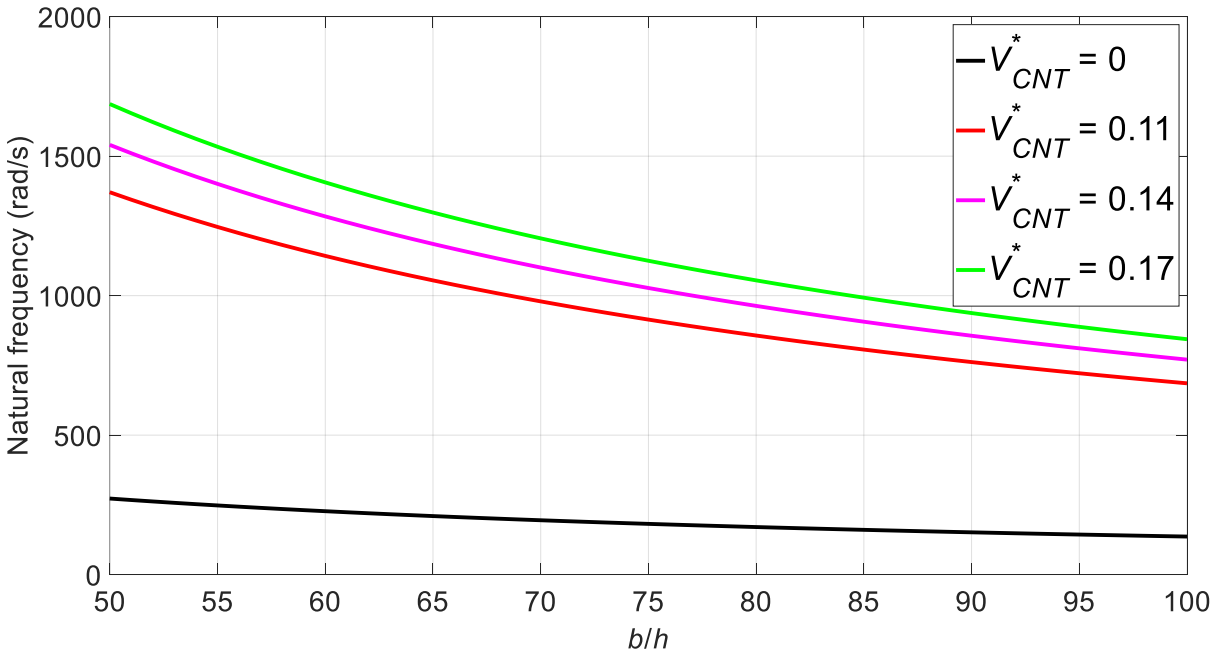

(d)

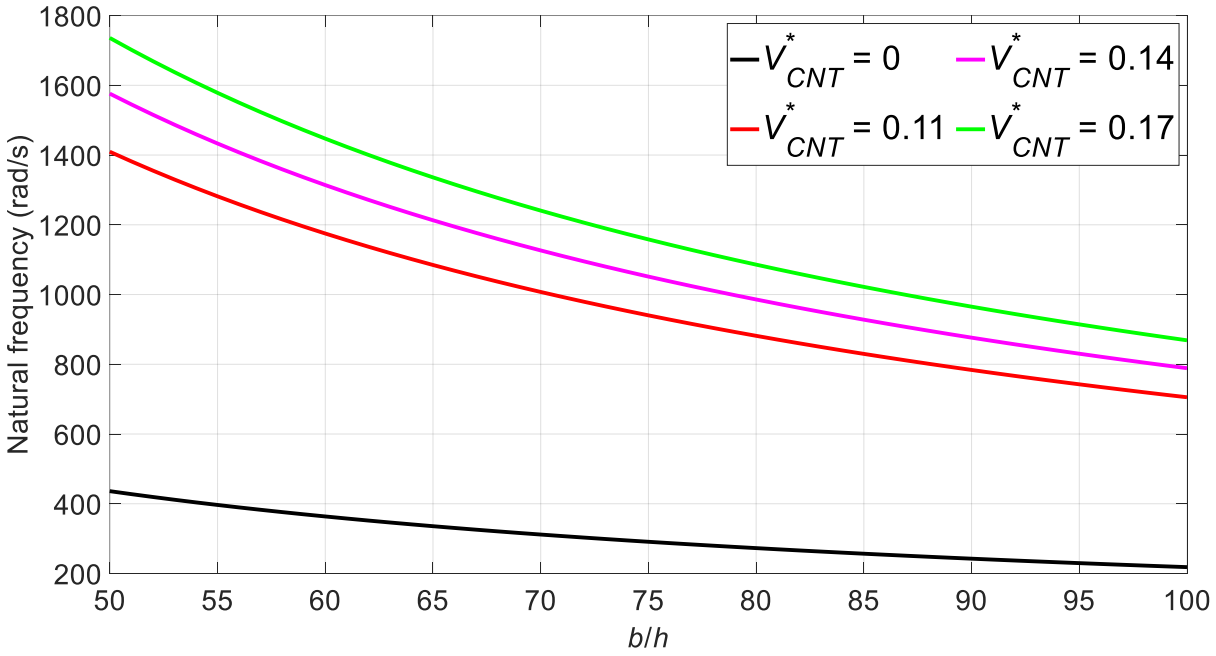

Fig. 10: Thickness effects on the *first* series dimensional transverse-motion natural frequencies of a UD carbon nanotubes reinforced square double plates, (a) $\omega_{1,11}$; (b) $\omega_{1,12}$; (c) $\omega_{1,21}$; (d) $\omega_{1,22}$.

(a)

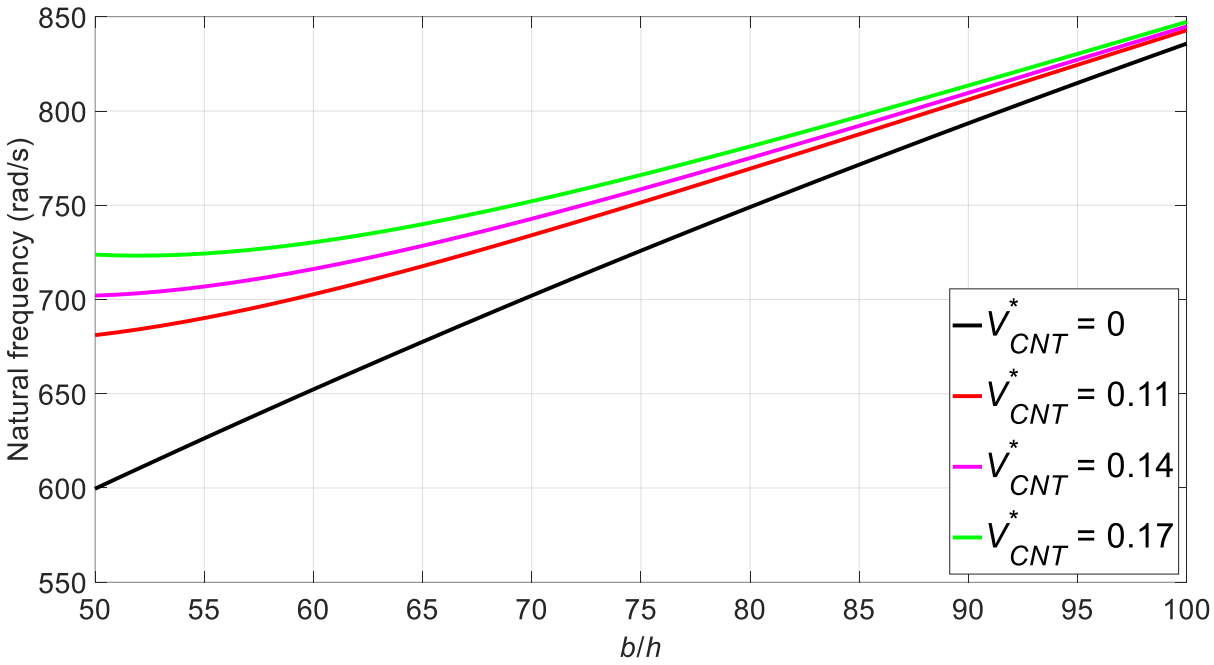
Natural frequency (rad/s)
850
800
750
700
650
600
550
50
55
60
65
70
75
80
85
90
95
100
b/h
V^*_{CNT} = 0
V^*_{CNT} = 0.11
V^*_{CNT} = 0.14
V^*_{CNT} = 0.17

(b)

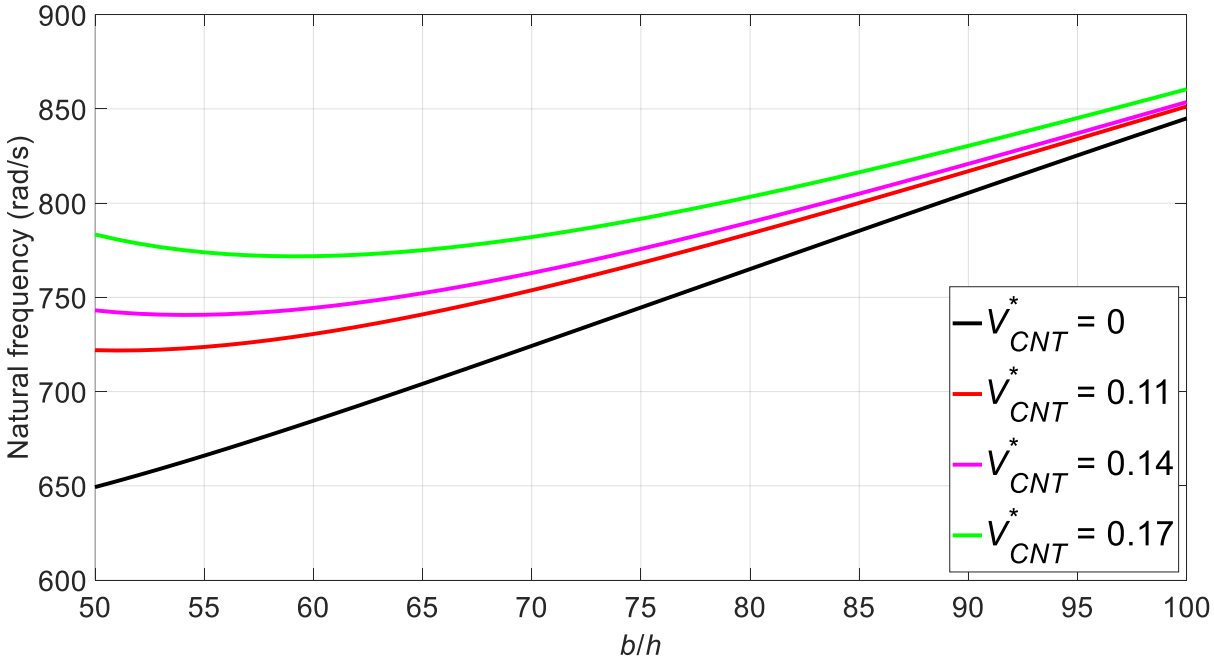
Natural frequency (rad/s)
900
850
800
750
700
650
600
50
55
60
65
70
75
80
85
90
95
100
b/h
V^*_{CNT} = 0
V^*_{CNT} = 0.11
V^*_{CNT} = 0.14
V^*_{CNT} = 0.17

(c)

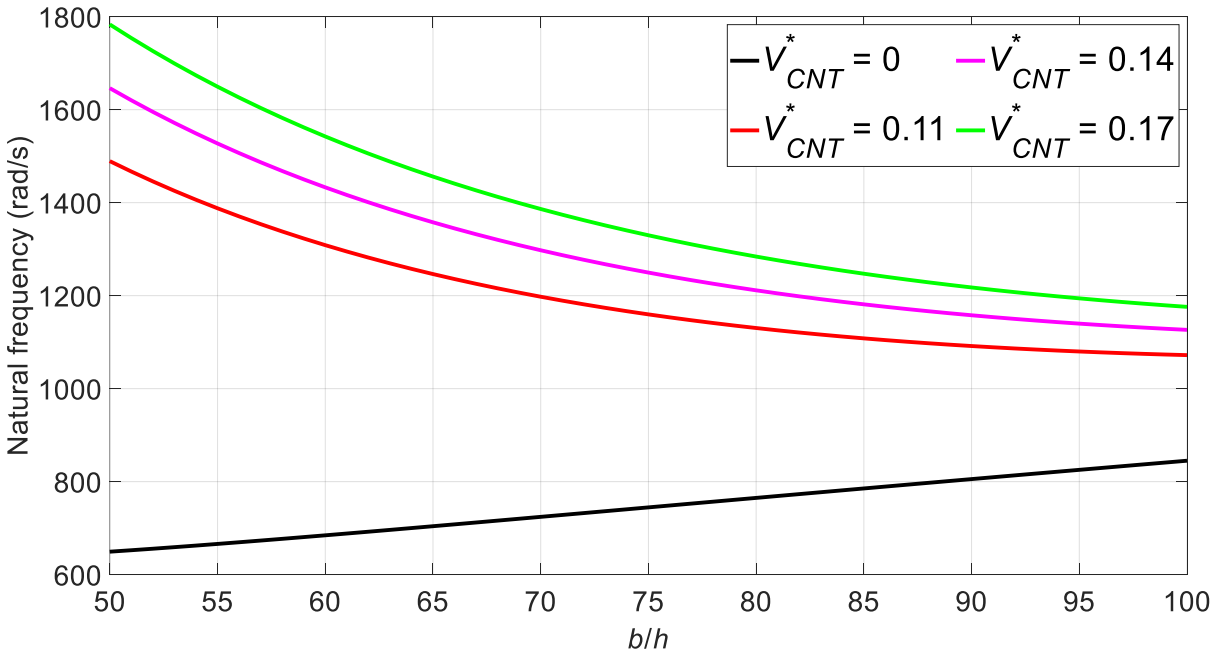

(d)

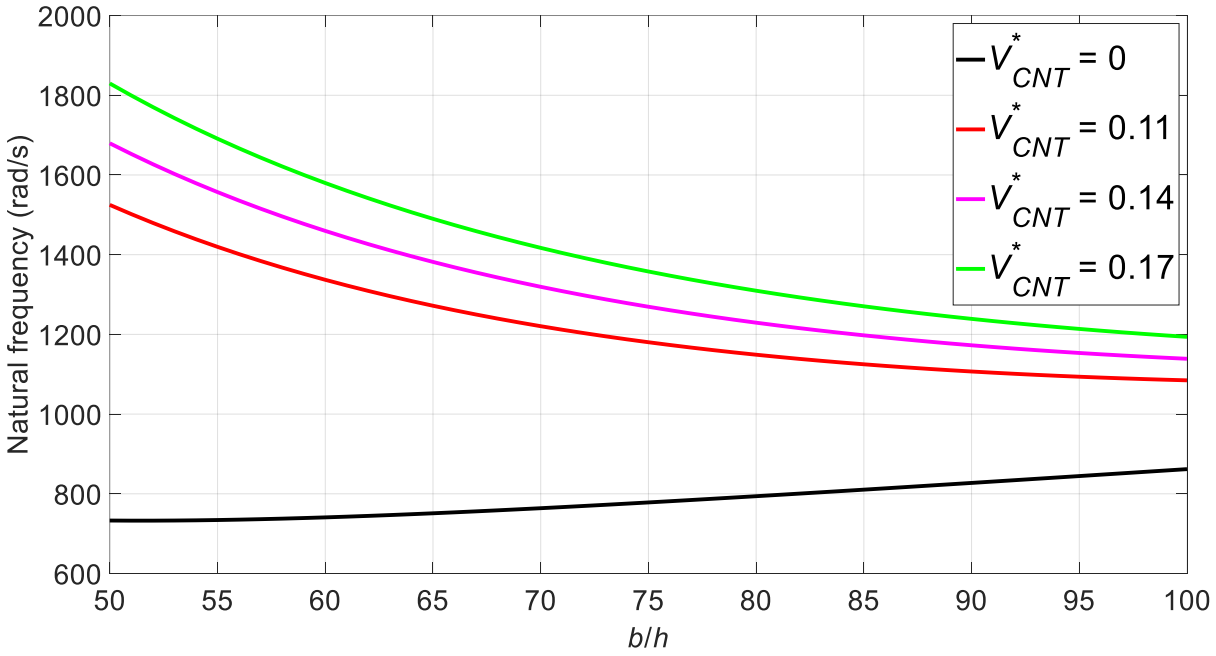

Fig. 11: Thickness effects on the *second* series dimensional transverse-motion natural frequencies of a UD carbon nanotubes reinforced square double plates, (a) $\omega_{2,11}$; (b) $\omega_{2,12}$; (c) $\omega_{2,21}$; (d) $\omega_{2,22}$.

(a)

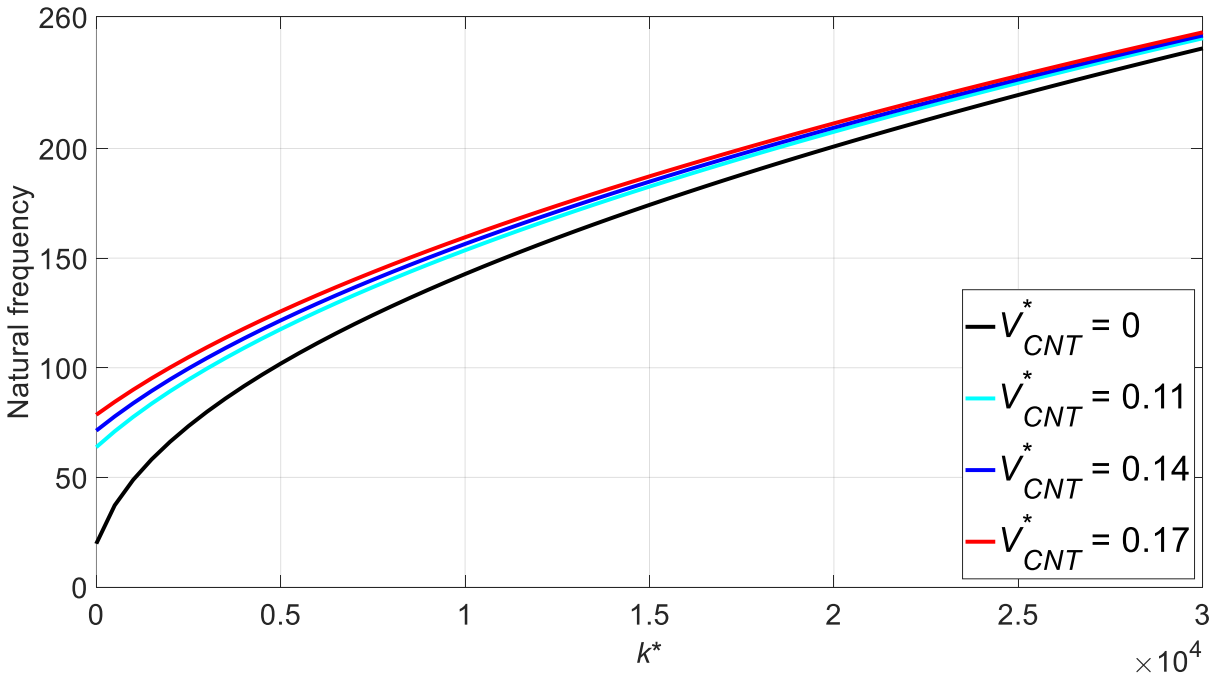
Natural frequency
260
200
150
100
50
0
0
0.5
1
1.5
2
2.5
3
k*
×10^4
V*CNT = 0
V*CNT = 0.11
V*CNT = 0.14
V*CNT = 0.17

(b)

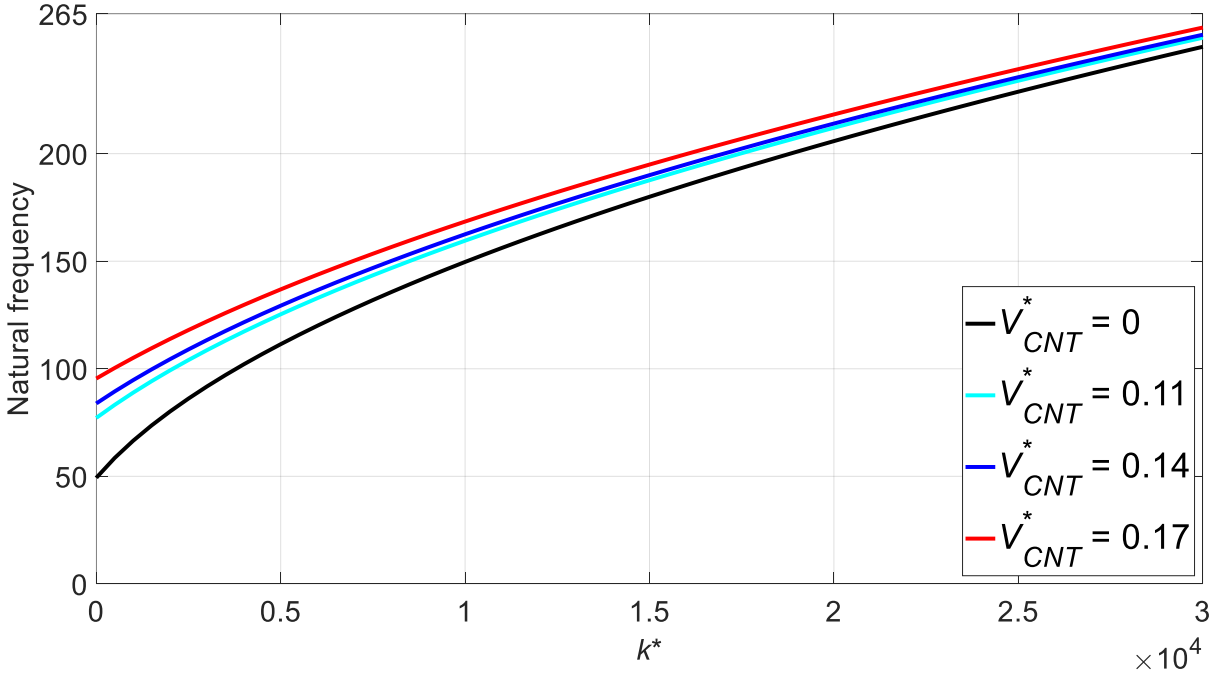
Natural frequency
265
200
150
100
50
0
0
0.5
1
1.5
2
2.5
3
k*
×10^4
V*CNT = 0
V*CNT = 0.11
V*CNT = 0.14
V*CNT = 0.17

(c)

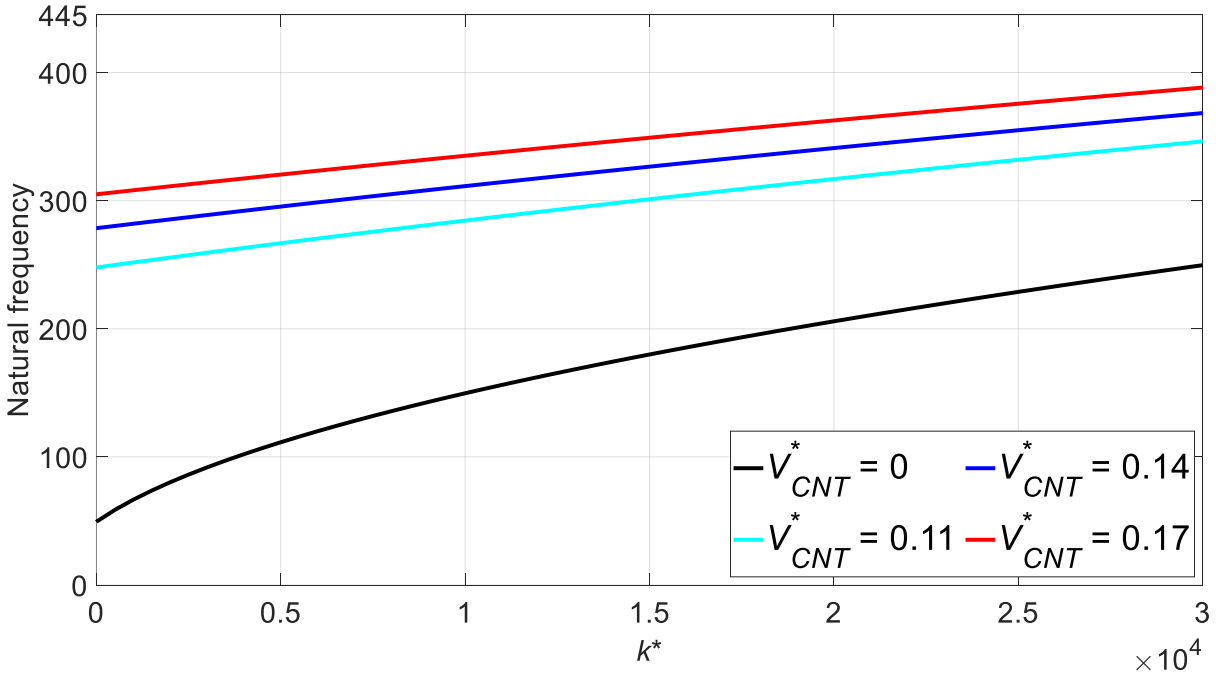

(d)

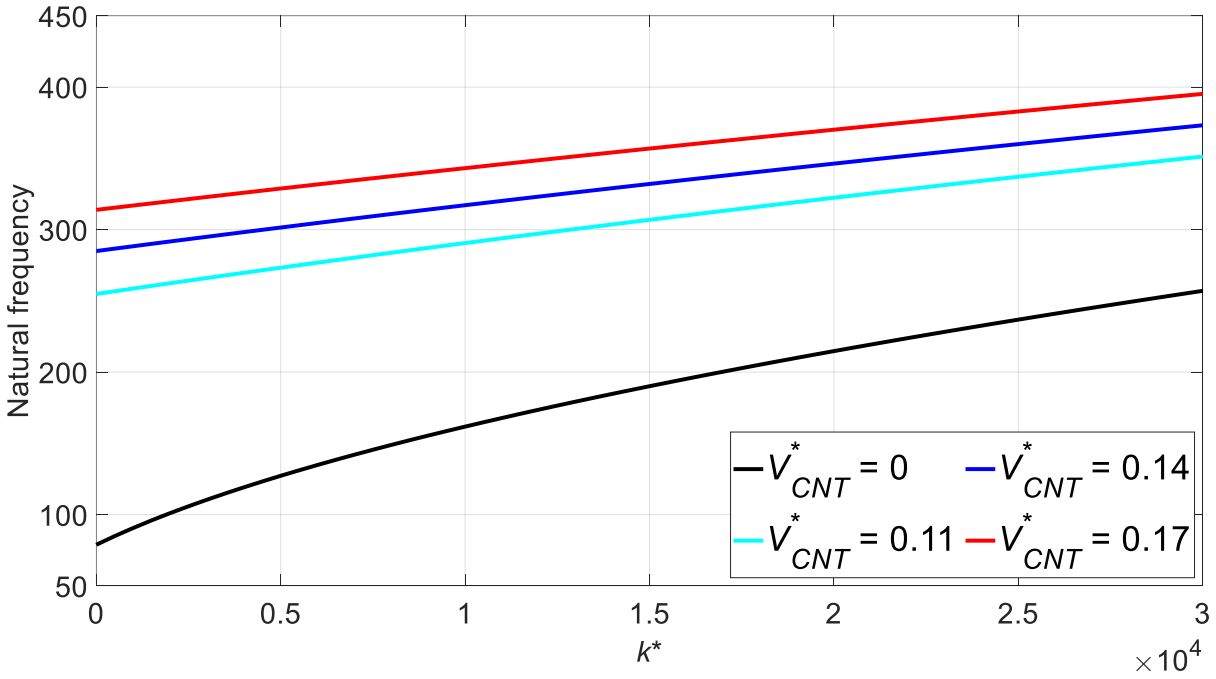

Fig. 12: Elastic layer stiffness effects on the *second* series dimensional transverse-motion natural frequencies of a UD carbon nanotubes reinforced square double plates, (a) $\omega_{2,11}$; (b) $\omega_{2,12}$; (c) $\omega_{2,21}$; (d) $\omega_{2,22}$.

(a)

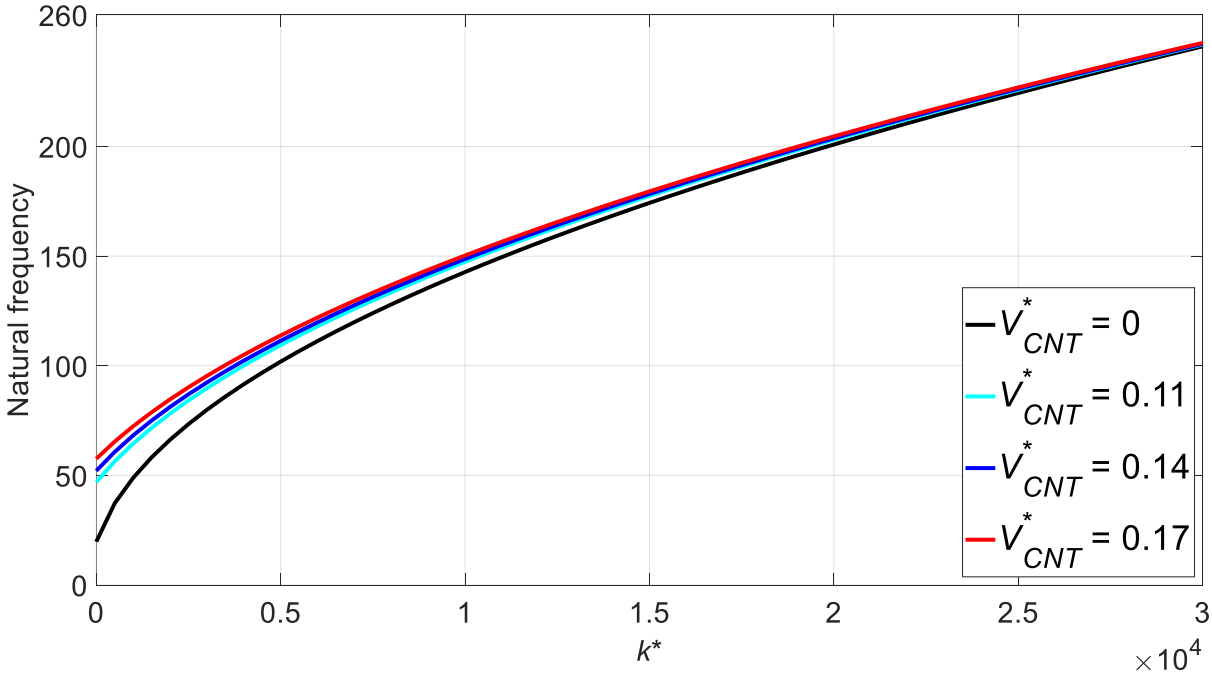
Natural frequency
260
200
150
100
50
0
0
0.5
1
1.5
2
2.5
3
k*
×10^4
V*CNT = 0
V*CNT = 0.11
V*CNT = 0.14
V*CNT = 0.17

(b)

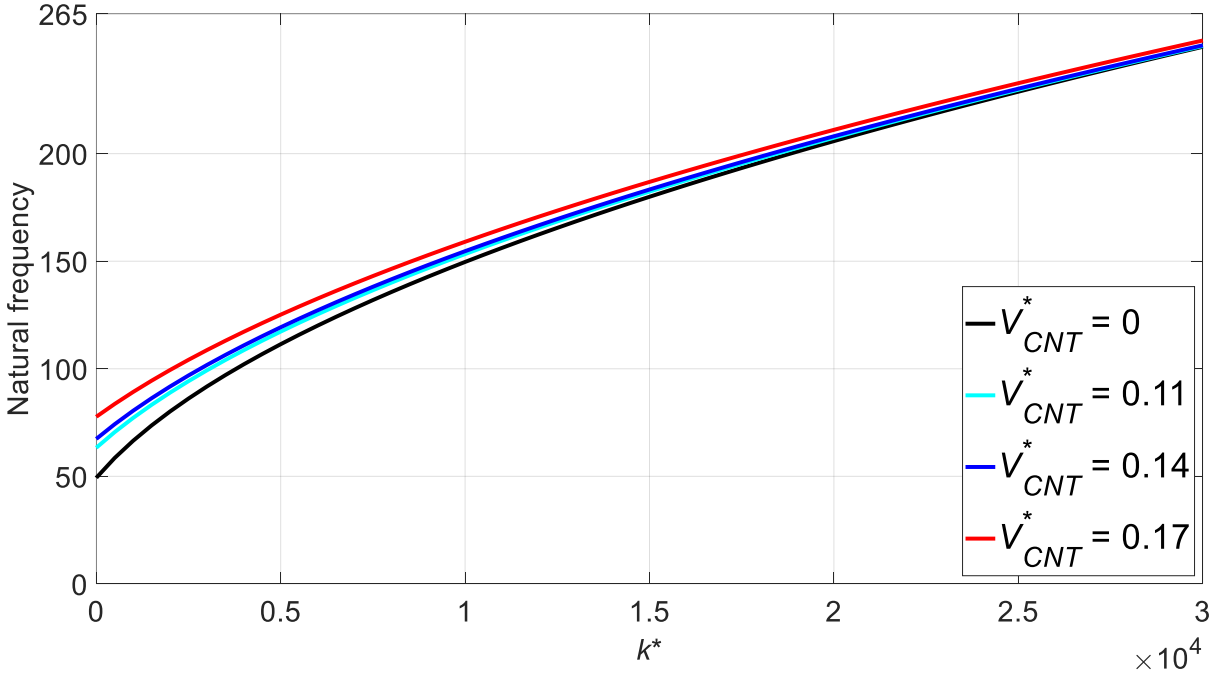
Natural frequency
265
200
150
100
50
0
0
0.5
1
1.5
2
2.5
3
k*
×10^4
V*CNT = 0
V*CNT = 0.11
V*CNT = 0.14
V*CNT = 0.17

(c)

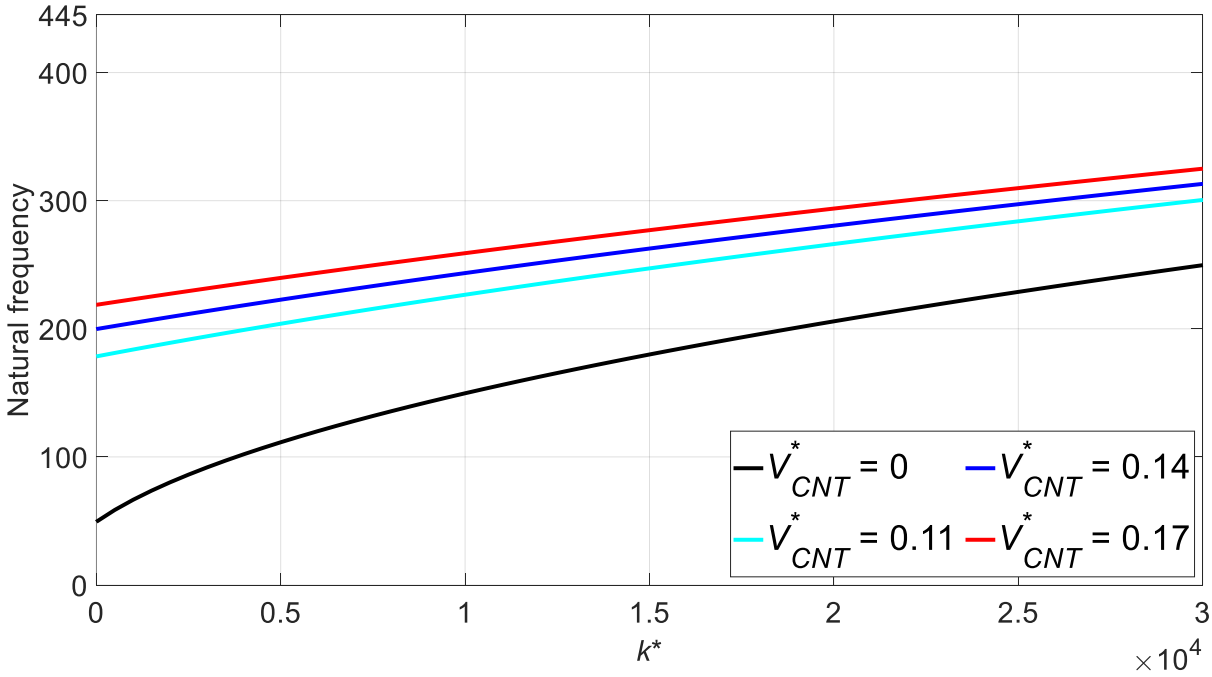

(d)

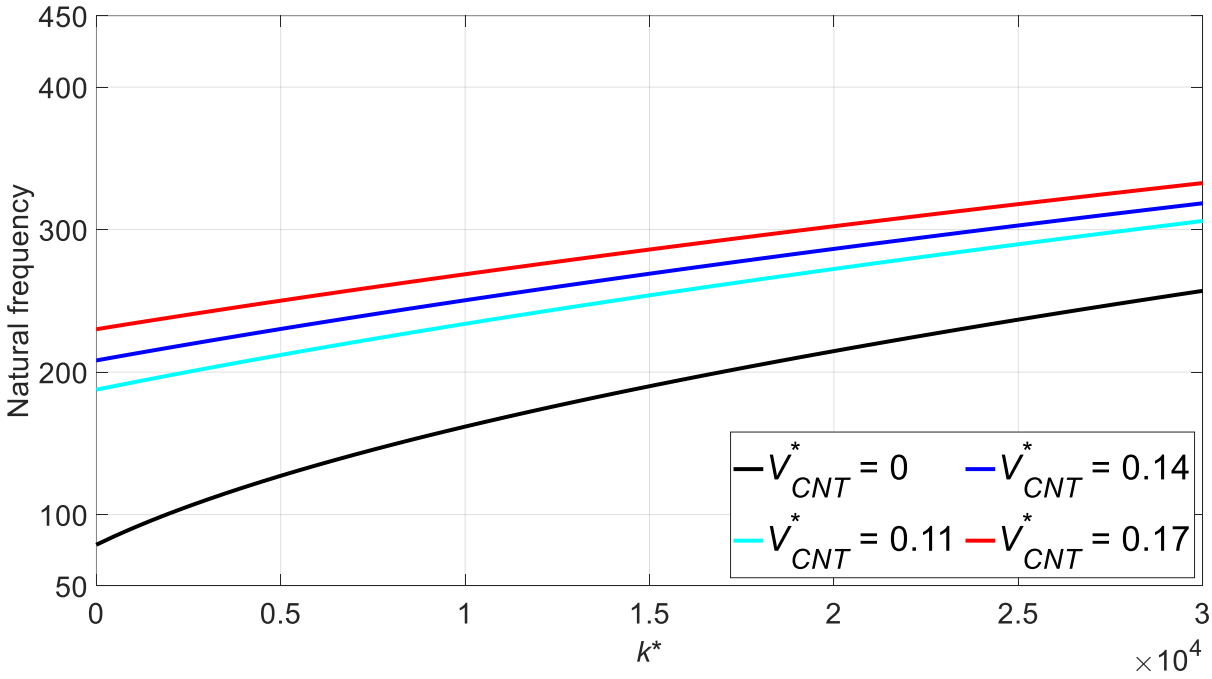

Fig. 13: Elastic layer stiffness effects on the *second* series dimensional transverse-motion natural frequencies of a FG-O carbon nanotubes reinforced square double plates, (a) $\omega_{2,11}$; (b) $\omega_{2,12}$; (c) $\omega_{2,21}$; (d) $\omega_{2,22}$.

(a)

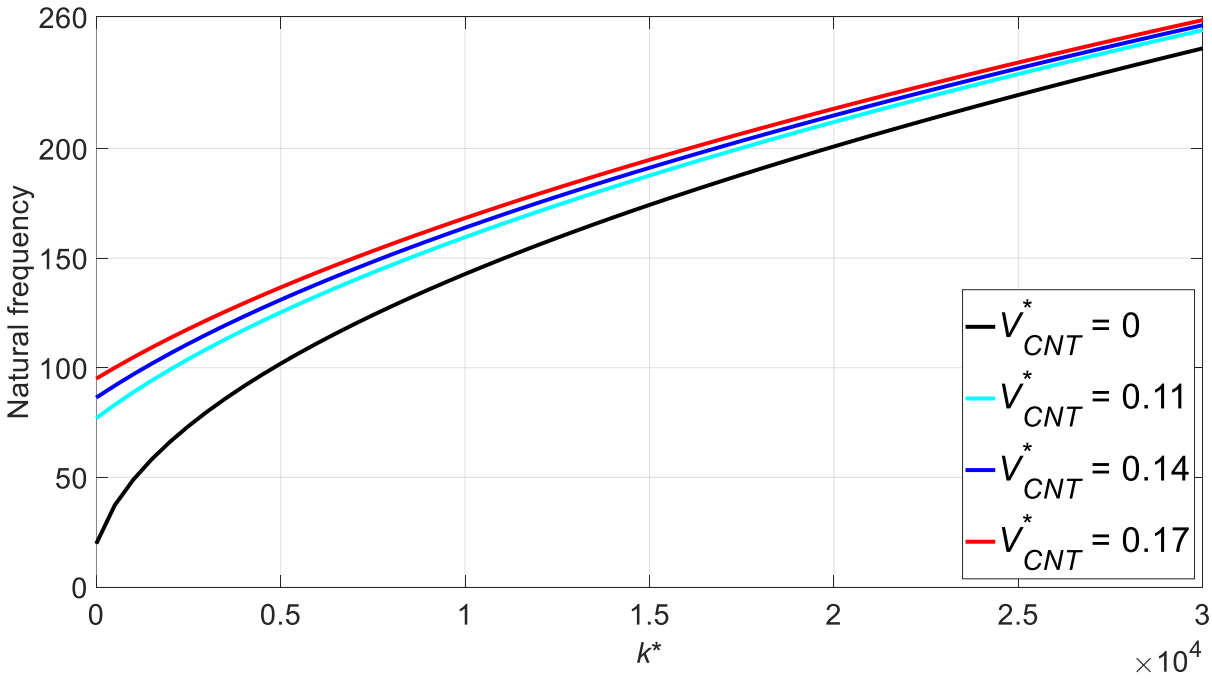
Natural frequency
260
200
150
100
50
0
0
0.5
1
1.5
2
2.5
3
k*
×10^4
V*CNT = 0
V*CNT = 0.11
V*CNT = 0.14
V*CNT = 0.17

(b)

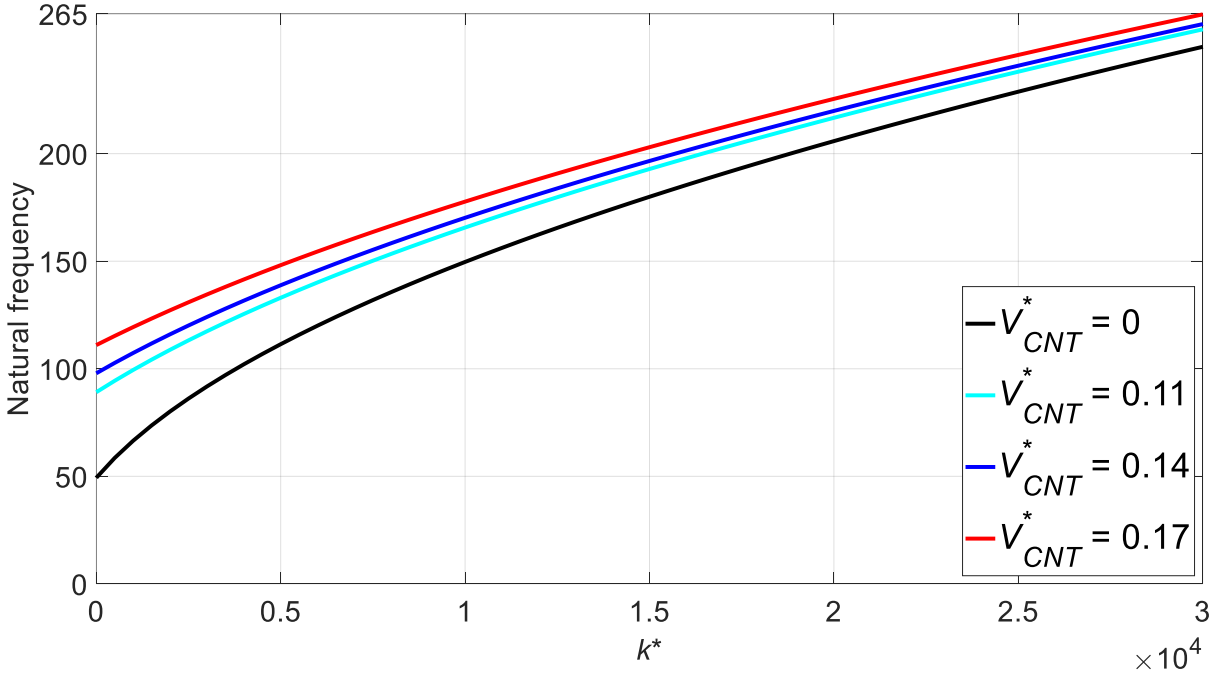
Natural frequency
265
200
150
100
50
0
0
0.5
1
1.5
2
2.5
3
k*
×10^4
V*CNT = 0
V*CNT = 0.11
V*CNT = 0.14
V*CNT = 0.17

(c)

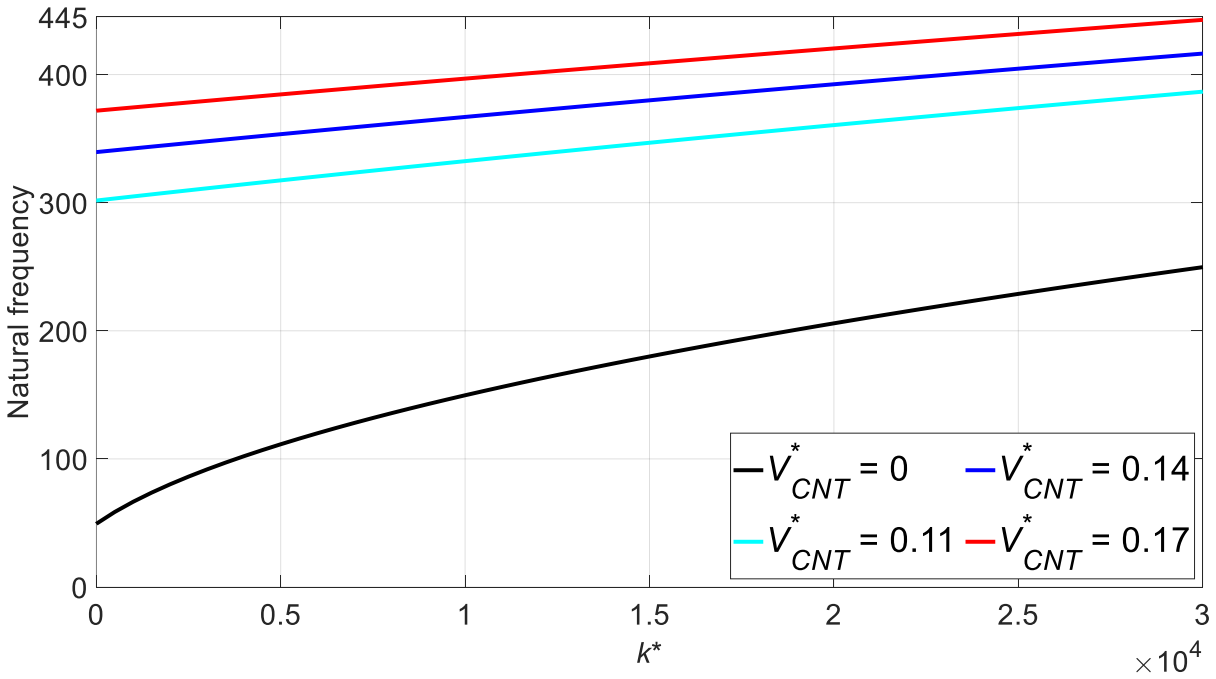

(d)

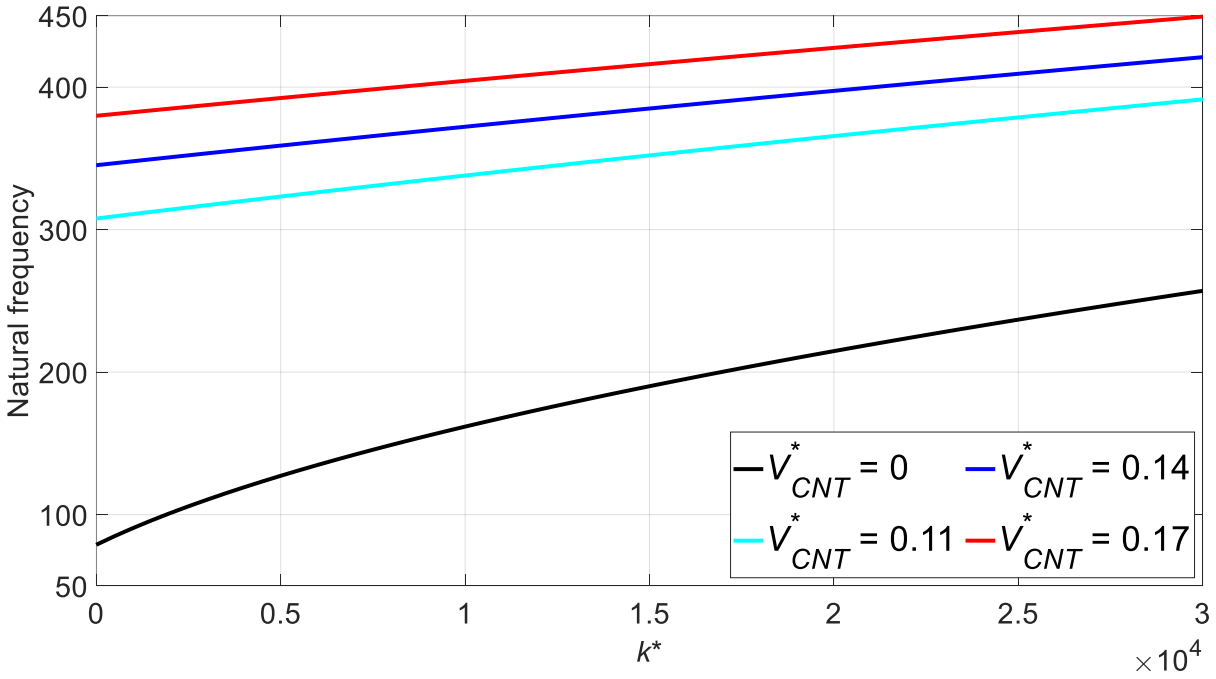

Fig. 14: Elastic layer stiffness effects on the *second* series dimensional transverse-motion natural frequencies of a FG-X carbon nanotubes reinforced square double plates, (a) $\omega_{2,11}$; (b) $\omega_{2,12}$; (c) $\omega_{2,21}$; (d) $\omega_{2,22}$.